Topological Phases and Families of Free Fermions

Sashank Chandra Reddy Singam

A thesis submitted for the partial fulfilment of the requirements for the BS-MS Dual Degree Programme

Indian Institute of Science Education and Research, Pune
Dr. Homi Bhabha Road
Pashan, Pune 411008, India

March, 2026

Supervisor: Abhishodh Prakash

Certificate

This is to certify that the dissertation entitled **"Topological Phases and Families of Free Fermions"**, submitted towards the partial fulfilment of the requirements for the **BS–MS Dual Degree Programme** at the **Indian Institute of Science Education and Research, Pune**, represents the work carried out by **Sashank Chandra Reddy Singam** under the supervision of **Dr. Abhishodh Prakash**, Department of Physics, Harish-Chandra Research Institute, Prayagraj, during the academic year **2025–2026**.

Abhishodh Prakash

Sashank Chandra Reddy Singam

Dissertation Committee:
Dr. Abhishodh Prakash
Dr. Sachin Jain

To all the colors of the world, and the morbid greys interspersed.

Declaration

I hereby declare that the matter embodied in the report entitled **Topological Phases and Families of Free Fermions** are the results of the work carried out by me at the Department of Physics, Harish-Chandra Research Institute, Prayagraj under the supervision of Dr. Abhishodh Prakash and the same has not been submitted elsewhere for any other degree.

Abhishodh Prakash

Sashank Chandra Reddy Singam

Acknowledgements

This thesis can be described as a consummation of the many people I have met and the span of my decisions throughout recent years. For I am but a lump of clay moulded by the many hands that grazed past, be it accidental or not.

It would be unacceptable for me not to thank Abhishodh first, my thesis supervisor, for being an incredibly patient and outgoing academic. It is his support that allowed me to mess up in many situations and correct them. I have learnt a lot from this endeavour, both in the realm of physics and otherwise. On this account, I would also like to thank Sayantan and Suraj for having meaningful (and sometimes not so meaningful) discussions and making research fun. Also, I would like to thank Advay, Rithwik, Aarya, Shubham, and Nehad for making my time at HRI positive.

I would like to wholeheartedly acknowledge Prof. Sreejith's impact on my approach to science. Throughout my semester projects with him, I have delved into many of my curiosities. The ample amount of time he has given me to nurture my way of reasoning would definitely go a long way in shaping me as an academician. His vast breadth of know-how is always inspiring.

I would now like to thank ma and dad for nourishing my curiosity and being a stable foundation I could lean on. I acknowledge my sister's snacks that she sometimes (reluctantly so) offered. Finally, I acknowledge Hemanth and bujji, my cousins, who this section would feel unfinished leaving out.

And now for IISER Pune, the time where I would describe as the most pleasant and nurturing. I would firstly like to acknowledge the guest house, which served as a base for my cardinal directions in the first few weeks of my time here. The main building and the LHC, for forgiving the limited time I have spent there. I would lastly like to acknowledge ITI road and co., where the shawarmas and soya chaap might not technically be the best, but they did feel so.

Of course, I will speak about the people, though it would fill my heart, eyes, and several hundred books for me to properly dress them with their flairs and whimsies, all of which I hope to carry to my grave.

I would like to thank Harsh for being the best roommate I could possibly have asked for, and always being a fresh beacon of light(-ning?). Of the people on campus for their thesis for howsoever long, I would especially like to acknowledge Yash, Deepika, Chetanya, Srijani, Anay, and Kavya for encouraging and holding onto my impulsive decisions. Deepika for always trying to keep me on track with work, although mostly in vain; Yash and Chetanya for always being there for a bout of COD. I would also like to acknowledge Srijani's violin lessons, movie accompaniments, and support during tiring laundry sessions.

Among many, many other things, I would like to thank Aparajita, Ishaan, Deep, Apoorva(a), Harsh, and Ameya for faithfully being a part of the little run club we had going on. Das, Seona, Jai, Kartik, and Abhinav, in conjunction to the others I have mentioned, I would like to thank for all the amazing horror movie and Among Us nights that we shared in my room or otherwise. Further, for encouraging my brief stints of volleyball and other sports which I hold dear, I would like to thank Chinmayee. Lastly, I would like to specially recognise Aparajita for always being there for me on a fruitfully difficult path of emotional maturity.

I would like to acknowledge the INSPIRE-SHE fellowship and the HRI visiting student fellowship for making my stay at HRI for my thesis possible. Lastly, I acknowledge all the curious for contributing to the huge pillar of discoveries and inventions that I stand on. On this account, 10% of this thesis is dedicated to Potocki.

AI Contributions Statement

This work was primarily human-created. AI was utilised to make stylistic edits, wording and paraphrasing. AI was prompted for its contributions. AI content was reviewed and approved. The following models were used: ChatGPT, and Perplexity Pro. These models were used in the following ways: literature survey and resource finding, rephrasing and restructuring statements originally made by the author to invoke better flow, bug fixing in codes originally written by the author, and stylistic changes to the LaTeX document involving font size, margins, etc.

Abstract

The first part of this thesis will involve reviewing some preliminaries on topological phases and families, and their modern classification schemes. For the first part, we then study phase diagrams of charge-conserving systems in the class 'A' of the Altland-Zirnbauer classification. We introduce topological textures permeating the phase diagram and discuss the global properties, including edge mode loci, of the same. We then show using field theoretic techniques that these properties are robust to perturbations. Further, using the suspension construction recipe owing to a conjectured classification, we build higher dimensional generalities of the well-known topologically non-trivial families of the Rice-Mele and Berry's model. We aim to connect this to the DDKS invariant introduced in prior work to characterise higher-dimensional topological families.

For the second part, we review some work and efforts on describing a subset of gapless topological phases: topological metals. We aim to introduce a semi-metal with novel edge mode structuring arising from a torsion invariant from the non-orientable nature of the Brillouin zone.

Contents

List of Figures

List of Tables

Chapter 1

Introduction

More is different [3] and as far as microscopic particles as concerned, this turns out to be a boon in terms of unraveling a phenomenally intricate structure embedded in the landscape of modern condensed matter physics. In particular, while the fundamental constituents of matter obey relatively simple quantum mechanical laws, their collective organization at macroscopic scales gives rise to qualitatively new phenomena that are not transparently encoded in the microscopic Hamiltonian. The passage from a few-body description to a many-body framework introduces an enormous enlargement of the Hilbert space, and with it, the possibility of emergent degrees of freedom, effective quasiparticles, and collective excitations whose dynamics are governed by principles distinct from those operative at the microscopic scale.

This hierarchical structure of physical laws naturally leads to the framework of effective field theories, wherein irrelevant microscopic details are systematically integrated out, leaving behind universal low-energy descriptions characterized by symmetry, topology, and locality [4]. Within this paradigm, phases of matter are not merely catalogued by the symmetry properties of their order parameters, but by global properties of the ground state wavefunction itself. Such a viewpoint compels us to regard the ground state not simply as a minimal-energy configuration, but as an object encoding nontrivial geometric and topological data in parameter space.

It is precisely in this sense that condensed matter systems serve as a fertile arena for the realization of abstract mathematical structures. Concepts originating in differential geometry and topology—such as fiber bundles, characteristic classes, and homotopy invariants—find concrete physical manifestations in the classification of quantum phases. The emergence of these structures is neither accidental nor decorative.

Owing to a vibrant collaboration between condensed matter physicists, mathematicians, and high energy physicists, there has been a steady yet instrumental increase in our understanding of so-called topological phases of matter [5, 6]. These are said to differ from the conventional ones, which are ordered through symmetry principles, by bringing into light a different type of order driven by quantum fluctuations as mentioned earlier. Although there has been remarkable recent literature on such Quantum Phase Transitions (QPTs) in dynamical settings [7], we will only be focusing on equilibrium phases of matter at $T = 0$. Consequently, most of our concerns will be on ground states of Hamiltonians.

One can subdivide this set of topological phases into two realms based on their entanglement patterns: Long Range Entangled (LRE) and Short Range Entangled (SRE) phases. Although the former harbors its own set of interests owing to its hosting of *anyons* [8], a large part of this thesis will be dedicated to looking at a subset of the latter called Symmetry Protected Topological (SPT) phases of matter. Perhaps the most famous set of examples of these are referred to as topological insulators which are time-reversal invariant systems with protected boundary modes [9, 10]. The bulk of such systems is insulating and the ground state is connected to the trivial product-state by a Finite-Depth Local Unitary (FDLU) circuit. The classification of these SPT (SRE) phases has been an instrumental breakthrough, showcasing the rich mathematical structures at play. The original classification done for free fermion systems [2, 11] has been now generalized into a robust conjecture claiming to classify all SRE phases in all spatial dimensions (refer to [12, 13, 14] and Section 1.2). for more details on the same. Further, in this thesis, we shall not consider any mention towards the very interesting recent progress on intrinsically gapless SPTs (igSPTs) or other variants of gapless topological phases. Note that this set is qualitatively different to what consists of *topological metals*.

Relatedly, one can define a *family* of states with non-trivial topological properties [15, 14, 13, 16, 17]. It has been famously conjectured by Kitaev [13, 18, 12] that the classification of such families parametrized by a space X is done by a generalized cohomology group structure. This allows us a whole slew of tools to tackle and properly define such states. We make use of these techniques in this thesis to construct and describe quantitatively some topological features of families of trivial phases. We propose higher dimensional generalizations to the base members of each distinct set which are the Rice-Mele and the Berry models.

In the superseding section (Chapter 3), we talk about the realm of topological metals, which have been a subject of deep interest as of recently due to robust surface states and transport properties.

Most of the original work done by the author as a part of this thesis permeates Chapter 2 and Chapter 3. The comprehensive nature of the appendix is to present the material in a clean and largely self-contained manner.

1.1 Phases of matter

For the sake of allowing further refinement, we shall start off with a sufficiently vague definition of a phase of matter.

Definition: *A set of states, described by a Hamiltonian $H(\vec{\lambda})$, where $\vec{\lambda}$ denote a set of parameters, are said to be in the same* ***phase*** *of matter as long as they can be connected by a path in the parameter space without encountering singular behavior (phase transition).*

A depiction of a (subset of the) parameter space with singular transition loci is known familiarly as the phase diagram. Here, according to the given definition, gas and liq-

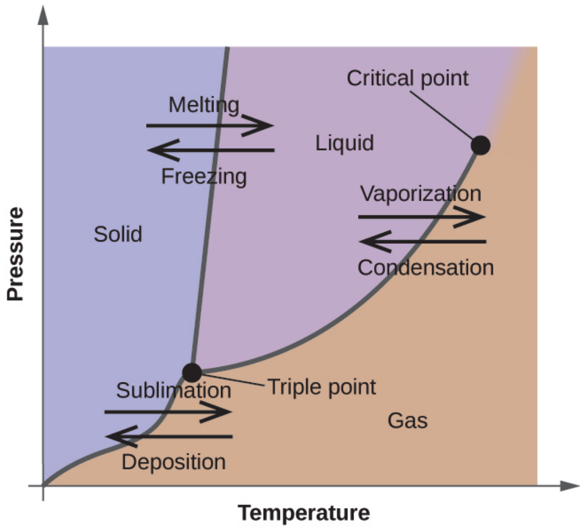

Figure 1.1: Phase diagram of water with the parameters being pressure and temperature.

uid regions belong to the same phase since one can find a path in the parameter space avoiding the transition line between the two. As an aside, there has been recent literature seeking to understand such *unnecessarily critical points* [19, 20]. However, if we don't have in handy the complete phase diagram (which generically is infinite-dimensional), to show that two regions don't belong to the same phase means showing that there exists *no* smooth path between them, which is an impossible ask. On this front, if one assigns to sets of Hamiltonians a quantity that doesn't change unless one crosses a singular region, the task reduces to calculating this invariant in the regions of interest. These are *topological invariants*. One such invariant is the ground state degeneracy of the Hamiltonian.

1.1.1 Landau's paradigm

Definition: *Say we are given a Hamiltonian $H(\vec{\lambda})$ which is $G-$symmetric, that is, $[U_g, H] = 0,\ \forall\ g\ \in G$ where U_g denotes a representation of the symmetry group. When $|\psi\rangle$ in the ground state subspace $\mathcal{H}_0$ of the total Hilbert space $\mathcal{H}$ respects a reduced symmetry group $H \subset G$, then we say that the symmetry is spontaneously broken into H.*

Then, the following statement can be made about the ground state degeneracy (GSD) for a Hamiltonian:

$$\text{GSD} \geq \frac{|G|}{|H|} \tag{1.1}$$

This can be seen as follows: say $g \in G/H$ and $|\psi\rangle \in \mathcal{H}_0$. For every such g, we have another state $|\phi\rangle := U_g|\psi\rangle$ for which

$$H|\phi\rangle = HU_g|\psi\rangle = U_gH|\psi\rangle = E_0U_g|\psi\rangle = E_0|\phi\rangle \tag{1.2}$$

A familiar example would be the Bose gas to superfluid transition which has to do with a $U(1)$ symmetry breaking, giving us gapless modes in terms of phonons. Using this line of reasoning, it was thought that spontaneous symmetry breaking explained all possible phases of matter. That is, until the discovery of the Integer Quantum Hall Effect (IQHE). This leads us straightforwardly into the following discussion.

1.2 Topological phases

The modern view of defining such phases is by a manner of distinction with respect to the "trivial" phases described before. The qualitative properties of topological phases are defined in terms of global topological invariants instead of a local order parameter that comes along with any description involving spontaneous symmetry breaking. One thing to note is that ground state degeneracy is also such a global invariant, although here, it turns out that a change in this can not be associated with a symmetry breaking principle (although there exist modern treatments claiming to describe this using a broader range of symmetries, that is, generalized higher-form or non-invertible symmetries). For this section, we will only concern ourselves with phases having a gap in the bulk.

Broadly, these phases can be subdivided into two classes. The first is denoted by intrinsic topological order: these systems have finite ground state degeneracy in the bulk when on a torus. On the other hand, there are systems whose ground state degeneracy is only manifest when the system is taken with open boundary conditions. Although the modern version of the classification can be conjectured for both of these categories as a whole, we start with the first of such attempts which singles out the latter type.

1.2.1 The tenfold way

One of the first breakthroughs in the understanding of the structure behind such phases was in the case of non-interacting fermions. This was first completed by [11] in a random matrix study where they identify four universality classes of matrices which are obtained after imposing T (time-reversal) and Q (particle-hole) symmetries. Including the earlier results of the three "chiral" Gaussian ensembles and more familiarly, the Gaussian Orthogonal Ensemble (GOE), Gaussian Unitary Ensemble (GUE), and the Gaussian Symplectic Ensemble (GSE), we get the celebrated tenfold way classification. However, this only really classifies quantum-mechanical systems completely. Although additional efforts have been made individually by [21, 22, 1], Kitaev unified all of these using a K-theoretic classification [2]. We review some of the crucial steps and assumptions in the following section.

Class	T	C	S	Time evolution operator $U(t) = e^{itH}$
A	0	0	0	$U(N)$
AI	+1	0	0	$U(N)/O(N)$
AII	-1	0	0	$U(2N)/Sp(2N)$
AIII	0	0	1	$U(N+M)/U(N)\times U(M)$
BDI	+1	+1	1	$SO(N+M)/SO(N)\times SO(M)$
CII	-1	-1	1	$Sp(2N+2M)/Sp(2N)\times Sp(2M)$
D	0	+1	0	$O(N)$
C	0	-1	0	$Sp(2N)$
DIII	-1	+1	1	$O(2N)/U(N)$
CI	+1	-1	1	$Sp(2N)/U(N)$

Table 1.1: Ten-fold way symmetry classes and associated symmetric spaces.

Using $K-$theory

$K-$theory primarily being a mathematical subfield focused on classifying vector bundles, makes its way into the realm of topological phases through some key ideas. The first of these is stable equivalence. This basically means that we can augment the system with additional (without loss of generality, trivial) bands without making a change to the overall classification (this makes sense since in physical systems, we have a very large number of bands).

$$X' \sim X'' \quad \text{if} \quad X' \oplus Y \sim X'' \oplus Y \tag{1.3}$$

This helps: it may be true that two systems in say, the phase diagram, are not deformable to each other directly, but such a deformation becomes feasible after the

Class	Simplified Hamiltonian
A	$\{\, Q(k) \in G_{m,m+n}(\mathbb{C}) \,\}$
AI	$\{\, Q(k) \in G_{m,m+n}(\mathbb{C}) \mid Q(k)^* = Q(-k) \,\}$
AII	$\{\, Q(k) \in G_{2m,2(m+n)}(\mathbb{C}) \mid (i\sigma_y)Q(k)^*(-i\sigma_y) = Q(-k) \,\}$
AIII	$\{\, q(k) \in U(m) \,\}$
BDI	$\{\, g(k) \in U(m) \mid g(k)^* = g(-k) \,\}$
CII	$\{\, q(k) \in U(2m) \mid (i\sigma_y)q(k)^*(-i\sigma_y) = q(-k) \,\}$
D	$\{\, Q(k) \in G_{m,2m}(\mathbb{C}) \mid \tau_x Q(k)^* \tau_x = -Q(-k) \,\}$
C	$\{\, Q(k) \in G_{m,2m}(\mathbb{C}) \mid \tau_y Q(k)^* \tau_y = -Q(-k) \,\}$
DIII	$\{\, q(k) \in U(2m) \mid q(k)^T = -q(-k) \,\}$
CI	$\{\, q(k) \in U(m) \mid q(k)^T = q(-k) \,\}$

Table 1.2: Classifying spaces for the ten Cartan symmetry classes after a 'spectral flattening' transformation, adapted from [1]. We refer to the same source for the technicality of what $q(k)$ means.

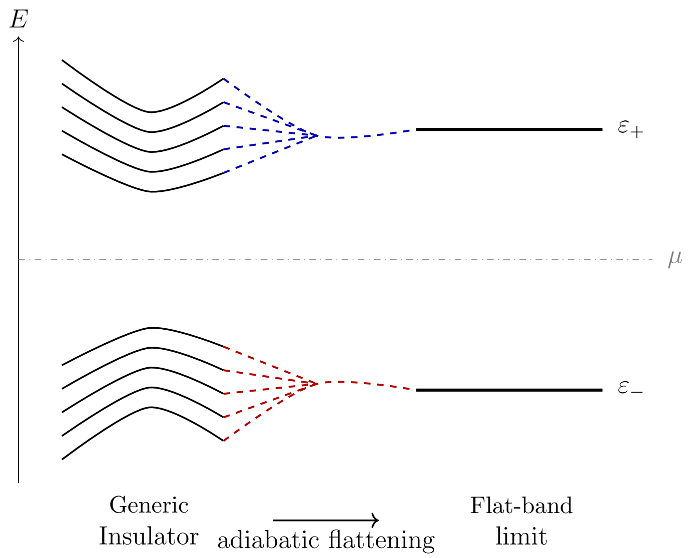

Figure 1.2: The 'spectral flattening' transformation of a generic admissible insulator.

augmenting with trivial bands. We also assume that the bands of the Hamiltonian are admissible, that is, the eigenvalues are bounded in both directions, and in such a case, there exists a flattening transformation as shown in Fig. 1.2. This allows us to construct the coset of distinct flattened Bloch Hamiltonians $Q(\vec{k})$. As one can see in Table 1.2, for the symmetry class A, the classifying space is given by the (complex) Grassmanian $G_{m,m+n}(\mathbb{C})$ (note that this is prior to using the stable equivalence property from before). However, doing the same for the other classes is very non-trivial due to constraints from the symmetry actions, and further, the structure is not fully transparent. On this account, adding the stable equivalence property, we cross over into the realm of (complex) $K-$theory where now the classifying space becomes:

$$C_0 = \bigcup_{k\in\mathbb{Z}} \lim_{s\to\infty} U(2s)/(U(s+k)\times U(s-k)) \tag{1.4}$$

Now, this leads to a simplification after convening with an equivalent extension problem involving the representations of the Clifford algebra [23]. Using this, for the real symmetry classes:

$$\pi(\bar{T}^d, R_q) = \pi_0(R_{q-d}) \oplus \bigoplus_{s=0}^{d-1} \binom{d}{s} \pi_0(R_{q-s}) \tag{1.5}$$

where R_q refer to the classifying spaces as mentioned in Table 1.3. This gives us the different ways that one can map the Brillouin zone (given by $\bar{T}^d$) onto the set of admissible Bloch matrices. Note: only the first piece on the RHS seems to be universal which stays along even for non-translational invariant systems. The ones characterized by the second part are called weak topological insulators (superconductors).

q mod 8	Classifying space R_q	$\pi_0(R_q)$
0	$(O(k+m)/(O(k)\times O(m)))\times\mathbb{Z}$	$\mathbb{Z}$
1	$O(n)$	$\mathbb{Z}_2$
2	$O(2n)/U(n)$	$\mathbb{Z}_2$
3	$U(2n)/Sp(n)$	0
4	$(Sp(k+m)/(Sp(k)\times Sp(m)))\times\mathbb{Z}$	$\mathbb{Z}$
5	$Sp(n)$	0
6	$Sp(n)/U(n)$	0
7	$U(n)/O(n)$	0

Table 1.3: Real classifying spaces R_q and their zeroth homotopy groups exhibiting Bott periodicity, adapted from the classification of topological phases by [2].

1.2.2 Bulk-boundary correspondence

Another equivalent way of performing the classification of free-fermion topological phases is owed to the principle of anomaly matching. This can be seen as a relatively straightforward, although still cumbersome, path to generalize to classify interacting topological phases. It relies on the fact that the boundary of a topological insulator (superconductor) cannot exist as a standalone system due to it being anomalous. This anomaly comes about through gauging a certain part of the symmetry group and is called a t' Hooft anomaly. The only way it can exist is as a part of a higher-dimensional bulk theory whose topological action has a boundary term which exactly *cancels* the one coming from the boundary modes.

The topological response term can be obtained by gauging a symmetry of the fermionic system at hand, and then integrating the fermions out. In the case of the system having no continuous symmetries, that is, if it lies in, say, the symmetry class D, we couple it to the gravitational field, obtaining a gravitational effective action. This leaves us with an effective action for the background fields (metric).

$$e^{-W_{eff}[A_\mu]} = \int \mathcal{D}[\bar{\psi}, \psi] e^{-S[\bar{\psi},\psi;A_\mu]} \tag{1.6}$$

This effective action can usually be divided into two parts: one pertaining to the usual (Maxwell-type) action, and a second topological response W_{eff} which only exists in the presence of a non-trivial boundary. These terms can be classified into (a) Chern-Simons type responses appearing in odd spacetime dimensions and (b) Theta-term type responses appearing in even. The familiar versions of these responses occur in 3 and 4 spacetime dimensions respectively:

$$W_{CS} = i\sigma_{xy} \int d^2x d\tau \frac{-1}{4\pi} \epsilon^{\mu\nu\lambda} A_\mu \partial_\nu A_\lambda \tag{1.7}$$

$$W_\theta = i\theta \int \frac{-1}{32\pi^2} \epsilon^{\mu\nu\kappa\lambda} F_{\mu\nu} F_{\kappa\lambda} d^3x d\tau \tag{1.8}$$

The essence of the anomaly cancellation (inflow) argument is that this topological response term is exactly canceled by the anomaly from the theory on the boundary. For example, chiral fermions in (1+1)D have a chiral anomaly function [24] which cancels the non-invariance of the boundary part of the Chern-Simons term coming from the higher-dimensional bulk. For a view on how this is done more generally, we refer to Chapter E

1.2.3 Generalised cohomology classification

Before we get onto the technicalities, we want to (re-)define some objects in a more rigorous manner. For some physical arguments and connections to other classification schemes, we refer to [12, 25].

Definition: *Given two systems r and s belonging to the same dimension, we define the composite system $r + s$ to be made by stacking s on top of r.*

Consider a symmetry group G. Now define $\mathcal{M}^d(G)$ to be the set of deformation classes of $d-$dimensional, gapped and local, G-symmetric, non-symmetry breaking systems. A deformation class can just be defined as an equivalence class of systems under the equivalence relation of deformation.

Definition: *A d-dimensional $G-$protected SPT phase is an invertible element of $\mathcal{M}^d(G)$. SPT phases are hence the invertible elements of the monoid $\mathcal{M}^d(G)$ under the operation of stacking defined before.*

Definition: *The non-invertible elements of $\mathcal{M}^d(G)$ are defined as Symmetry Enriched Topological (SET) phases; these consist of Long Range Entangled (LRE) phases and possess anyonic excitations in the bulk.*

Now for the conjecture:

Generalized Cohomology Hypothesis: *Given any dimension d and symmetry group G, there exists an (unreduced) generalized cohomology theory h such that $h^d(BG)$ classifies all $d-$dimensional G-protected SPT phases.*

Note

In the literature, different definitions of SPTs, SREs, LREs, intrinsic topological order and SETs are often used. We want to clarify the distinction between these and the one that we would use.

SREs are generally defined as local, gapped systems that can be deformed to a trivial one via Finite-Depth Local Unitary (FDLU) circuits. Note that this has no regards to symmetry and could involve symmetry breaking perturbations as well.

SPT phases are sometimes defined as a subset of SRE phases in the sense that they can also be deformed to a trivial state when symmetry breaking perturbations are allowed. They have a gap in the bulk with a unique ground state on closed manifolds although harboring gapless edge modes when put on a manifold with a boundary.

An interesting example is that of the Integer Quantum Hall (IQH) state which is topological, that is, harbors chiral gapless edge modes, but doesn't require any symmetry protection. So, it is a non-trivial SRE but not an SPT phase.

LRE phases and those showcasing intrinsic topological order mostly describe the same set: those which are gapped fully with a degeneracy when put on a torus. They house anyonic (fractional) excitations. Symmetry Enriched Topological (SET) phases share the same placement in LRE phases that SPT phases share with respect to the SRE ones.

1.3 Topological families

Using Fig. 1.1 as a reference point, are there questions one can ask about the structure of the phase diagram in its entirety? Is there a way to rigorously analyse the global skeleton of a specific phase diagram? We motivate these queries by introducing some examples. Note: whenever we talk about topological families, we take into consideration only gapped Hamiltonians with unique ground states. Hence, one can talk about *families of states* arising from corresponding families of Hamiltonians.

1.3.1 Spin-$\frac{1}{2}$ in a magnetic field

We analyse the following Hamiltonian describing a spin in the presence of a constant magnetic field which is parametrized by values $\in S^2$. Note that $\mathbb{R}^2$ is the entire phase diagram after taking B into consideration as a parameter.

$$H = \vec{B} \cdot \vec{\sigma} = B \begin{pmatrix} \cos\theta & e^{-i\phi}\sin\theta \\ e^{i\phi}\sin\theta & \cos\theta \end{pmatrix} \tag{1.9}$$

In this case, the set of ground states is again parametrized by points on S^2.

$$|-;\theta,\phi\rangle = \begin{pmatrix} e^{-i\phi}\sin\frac{\theta}{2} \\ -\cos\frac{\theta}{2} \end{pmatrix} \tag{1.10}$$

There is a certain non-triviality associated with this family of states. This can be seen by looking at $\theta = \pi$. Here, the state becomes:

$$|-\rangle = \begin{pmatrix} e^{-i\phi} \\ 0 \end{pmatrix} \tag{1.11}$$

where the angular coordinate isn't well defined: we have a multi-valued wavefunction at the south pole. One can in fact get rid of this ambiguity by making a gauge transformation $|-\rangle \to e^{i\phi}|-\rangle$. However now, the state at $\theta = 0$ becomes multi-valued. In general, it turns out that there is no single gauge choice one can associate with the whole manifold of states.

Viewing the set of ground states as a line bundle, this *obstruction* can be understood by a non-vanishing of the Chern number belonging to the first Chern class $\omega \in H^2(S^2, \mathbb{Z})$.

Now, we have an additional quantity that can be associated with a given phase diagram: the Chern number, which tells you if the family of states under consideration is trivial or not.

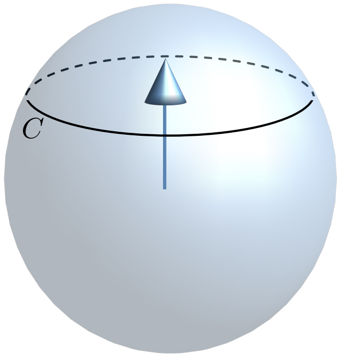

Figure 1.3: Berry's problem of a spin in a magnetic field. We look at a set of Hamiltonians parametrized on a sphere.

Turns out that there is a way to compute this quantity. First, we define the Berry connection,

$$\mathcal{A}_\mu(\theta, \phi) = \langle - | \partial_\mu | - \rangle \tag{1.12}$$

which is a geometric invariant that is well-defined as an angle $\gamma \in \mathbb{R}/2\pi\mathbb{Z}$. Correspondingly, the Berry curvature can be defined as follows,

$$\mathcal{F}_{\mu\nu} = \partial_\mu \mathcal{A}_\nu - \partial_\nu \mathcal{A}_\mu \tag{1.13}$$

Lastly, the Chern number is given by

$$\mathsf{C}_1 = \frac{1}{4\pi} \int \mathcal{F} d\lambda_1 \lambda_2 \tag{1.14}$$

where the integral is over the family denoted by the set of parameters $\vec{\lambda} = \{\lambda_1, \lambda_2\}$. It can be argued that Eq. (1.14) gives a quantized number and in the case in consideration, upon explicit computation, we get 1.

Diabolical loci

Turns out equally important is the fact that there exists a gap touching at $B = 0$. Such points in the phase diagram are called diabolical loci $\mathcal{D}$ which *source* the non-trivial topology around them. It is clear to note that the Berry curvature has a monopole singularity at $\mathcal{D}$ in the previous example. However, things get further complicated when dealing with many-body systems and the diagnosis of truly diabolical loci is not trivial. For more details on this, we refer to 2[15].

Chapter 2

Topological Textures

Our aim of this chapter would be to showcase illustratively with explicit models some of the topological structures previously mentioned in Section 1.3 and also introduce some new ones which we call *topological textures*. We will do so using two distinct series of topological families: the thouless pump and the aforementioned Berry's model. Both of these reside in the class A of the Altland-Zirnbauer classification with a $U(1)$ symmetry; any other symmetries will be considered accidental. We shall construct higher dimensional generalizations of the previously known models in each set using the suspension construction, which will be introduced in Chapter D, and extend the structures discussed. We will further notice that this is in line with Kitaev's conjecture of a generalized cohomology classification of invertible states in a general spatial dimension.

2.1 The Rice-Mele model

To start off the first series, we will look at the following model of non-interacting spinless fermions on a 1-dimensional lattice with staggered hopping amplitudes and chemical potentials, defined by

$$\mathrm{H}_{\mathrm{RM}} = \sum_{x\in\mathbb{Z}} t_x \left(c^\dagger(x)c(x+1) + h.c\right) + \sum_{x\in\mathbb{Z}} \mu_x n(x) \tag{2.1}$$

$$t_x = \frac{(1+(-1)^x\delta)}{2}, \;\; \mu_x = \mu + (-1)^x J. \tag{2.2}$$

We restrict the parameters to the range $J \in (-\infty, \infty)$, $\delta \in [-1, 1]$. Eq. (2.1) has a two-site translation symmetry T and a charge conservation $U(1)$ symmetry that act as

$$\mathrm{T}_x : c(x) \mapsto c(x+2), \;\; \mathrm{U}(1) : c(x) \mapsto e^{i\vartheta}c(x) \tag{2.3}$$

First, consider the $\mu = 0$ limit of the model. Analogous to the SSH model [26], we can define a two-site fiducial unit cell. This can be seen in Fig. 2.1. In the momentum

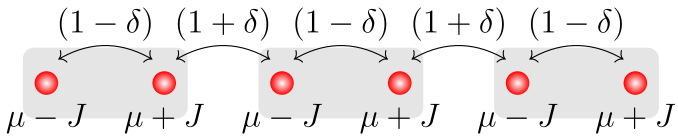

Figure 2.1: The Rice-Mele model with a two-site fiducial unit cell

space, we get

$$\mathrm{H}_{\mathrm{RM}} = \sum_k \sum_{\alpha,\beta} d^{\dagger}_{\alpha}(k)\mathrm{h}_{\alpha\beta}(k)d_{\beta}(k). \tag{2.4}$$

where the Bloch Hamiltonian is given by

$$\mathrm{h}(k) = \mu\mathbb{1} + \vec{g}(k)\cdot\vec{\sigma} \tag{2.5}$$

where, $\vec{\sigma} = \{\sigma^1, \sigma^2, \sigma^3\}$ are the standard Pauli matrices and

$$\begin{aligned} g_1(k) &= \frac{(1-\delta)}{2} + \frac{(1+\delta)}{2}\cos k, \\ g_2(k) &= \frac{(1+\delta)}{2}\sin k, \;\; g_3(k) = -J. \end{aligned} \tag{2.6}$$

The dispersion relation of this model is Dirac-like at the origin of the parameter space and gapped everywhere else, see Fig. 2.2. Thus, the phase diagram just contains a

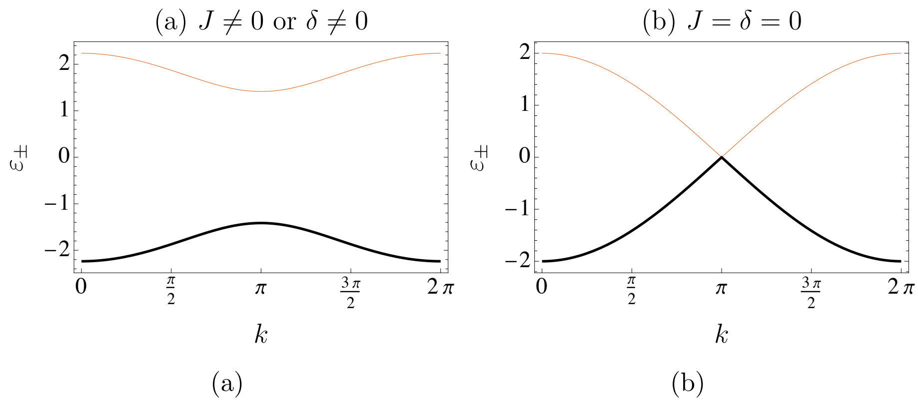

Figure 2.2: Dispersion of single-particle energies of Eq. (2.1) (a) away from and (b) at the origin of the J-δ plane. The gap closes only at the origin and remains open elsewhere.

single gapless point at the origin surrounded by a trivial band insulator. For finite chemical potential ($|\mu| < 1$) however, the gapless point blows up into showcasing a gapless disc with a radius equal to μ. This can be seen in Fig. 2.4. For $|\mu| > 1$, as shown in Fig. 2.4(c) the gapless phase splits into two disks and opens up an insulating phase in between, characterized by both bands being either fully filled or empty depending on the sign of μ. Although the various insulating regions are topologically trivial as phases, we will argue that the region with a single filled band (henceforth referred to as single-band insulator) has hidden topological features.

2.1.1 Topological features

In the case where we have the one-band insulator phase, for each point on the parameter space, one can define the Bloch-Berry connection to be

$$\mathcal{A}_k := -i\langle u_k|\partial_k|u_k\rangle \tag{2.7}$$

where $|u_k\rangle$ is the eigenstate describing the filled lower band. We get a geometric invariant by integrating this over the Brillouin zone which is $\sim S^1_{BZ}$.

$$\gamma(J,\delta) := \int_{S^1_{BZ}} \mathcal{A}_k dk \tag{2.8}$$

This gives us a $U(1)$ phase $\in [0, 2\pi]$. It is useful to consider the unit vector $\hat{g} = \vec{g}/|\vec{g}|$ which defines a map $\hat{g} : S^1_{\mathrm{BZ}} \to S^2$. The expression in Eq. (2.8) can be recast in terms of $\hat{g}$ as the solid angle Ω subtended over the target space unit sphere as shown in Fig. 2.3.

$$\gamma(J,\delta) = \frac{1}{2}\int_{k\in BZ} \frac{\hat{g}_x\partial_k\hat{g}_y - \hat{g}_y\partial_k\hat{g}_x}{1+\hat{g}_z}dk = \frac{1}{2}(\Omega) \tag{2.9}$$

To calculate this, since we are working with a unit sphere, it is proportional to the ratio of the area enclosed by the loop to that of the entire sphere. Finding this area itself is nontrivial. We do so using the Gauss-Bonnet theorem:

$$A(M) = 2\pi\chi(M) - \int_{\partial M} k_g ds \tag{2.10}$$

where χ is the characteristic number of the manifold (note that in the case of a submanifold of the sphere, or a disk, this is 1). Also, k_g is the extrinsic curvature of the loop from being embedded on the sphere:

$$k_g = \frac{\hat{g}''(k)\cdot(n\times\hat{g}'(k))}{||\hat{g}'(k)||^3} \tag{2.11}$$

where n is the normal to the surface. Plotting this angle along the $J-$axis, we get a vector for every point on the region described by the trivial insulator phase in the phase diagram. We call this the topological texture on the phase diagram.

This structure turns out to be stable, as we will see using Bosonisation and other field-theoretic techniques in Chapter B. This points to a topologically non-trivial family of states which can be diagnosed by computing the Chern number. To do so,

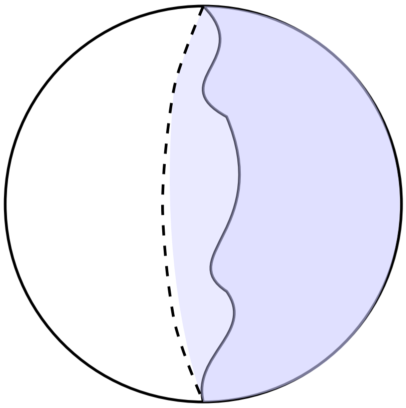

Figure 2.3: The image of $\hat{g}$ mapping the BZ at an illustrative parametric point (J, δ) to a closed curve on S^2. The colored cap denotes $\hat{g}(\bar{\mathcal{M}}_2)$ whose boundary gives us $\hat{g}(\partial\bar{\mathcal{M}}_2) = \hat{g}(S^1_{BZ})$ which is the domain of integration, by Stokes' theorem, for computing the Berry phase.

first we define the Berry connection valued on both the parameter values and the Brillouin zone,

$$\mathcal{A}_\mu(J, \delta, k) = -i\langle u_k(J, \delta)|\partial_\mu|u_k(J, \delta)\rangle \tag{2.12}$$

where μ takes values from $\{J, \delta, k\}$. Now consider any circle S^1_{par} surrounding the origin belonging to the gapped trivial phase (say, $J^2 + \delta^2 = c^2$ for $\mu < c < 1$), parametrized by θ and compute the first Chern number defined as the integral of the Berry curvature $F = \epsilon^{\mu\nu}\partial_\mu A_\nu$ over the two-dimensional manifold, $\mathcal{M}_2 = S^1_{\text{BZ}} \times S^1_{\text{par}}$

$$\mathsf{C}_1(\mathcal{M}_2) = \frac{1}{2\pi}\oint_{S^1_{\text{BZ}}} dk \oint_{S^1_{\text{par}}} d\theta F(k, \theta) \in \mathbb{Z} \tag{2.13}$$

The unit vector $\hat{g} = \vec{g}/|\vec{g}|$ defined earlier now produces a map $\hat{g} : \mathcal{M}_2 \to S^2$. Evaluating Eq. (2.13) is equivalent to computing the winding number of $\hat{g}$

$$\mathsf{C}_1(\mathcal{M}_2) = \frac{1}{4\pi}\oint_{S^1_{\text{BZ}}} dk \oint_{S^1_{\text{par}}} d\theta\ \hat{g} \cdot (\partial_k\hat{g} \times \partial_\theta\hat{g}). \tag{2.14}$$

For any parametric circle surrounding the origin of the phase diagram, Eq. (2.14) evaluates to $\mathsf{C}_1 = 1$. Since this is a topological invariant, any small deformation of the loop preserves it. If the parametric circle is subjected to a large deformation such that it no longer encloses the origin, it evaluates to $\mathsf{C}_1 = 0$. However, at some stage of the deformation when the circle touches the origin, the gap closes and Eq. (2.14) becomes ill defined.

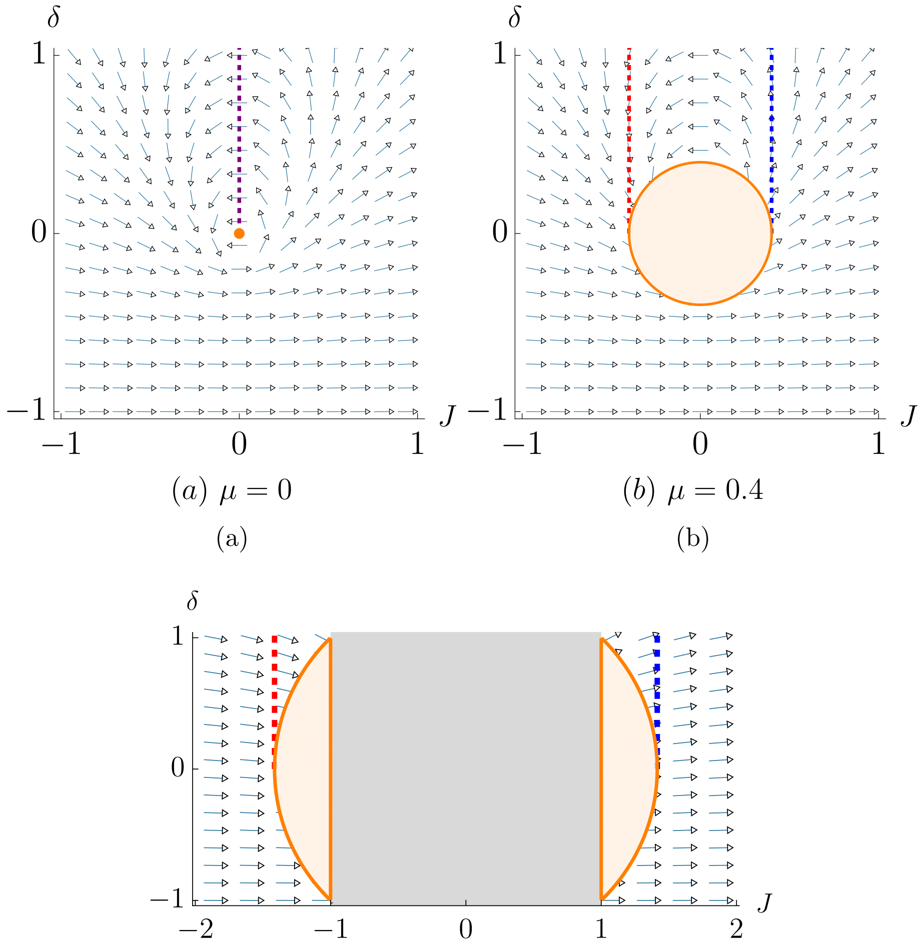

$(a)\ \mu = 0$

(a)

$(b)\ \mu = 0.4$

(b)

$(c)\ \mu = \sqrt{2}$

(c)

Figure 2.4: The phase diagrams of the Rice-Mele model shown in Eq. (2.1). The insulating phase with a single filled band has a topological texture similar to that of a vortex, exposed by plotting the Berry phase. The insulator with both bands filled or empty has no texture. The broken line indicates the presence of edge modes. For $\mu \neq 0$, the left and right edge modes occur on different parts of the phase diagram as can be seen in $(b), (c)$.

We have seen that the non-vanishing of the Chern number notified us about something non-trivial with the corresponding set of states. In this case, it indicates the presence of the Thouless pump [27, 28]. To see this, one can look at the periphery of the phase diagram given in Fig. 2.5. Tracing the charge at the boundary, one can think of a charge getting pumped to the boundary everytime we take a path around the origin. This can be tracked by calculating the boundary polarization with each parametric point which again turns out to be the corresponding Berry phase. The expression for

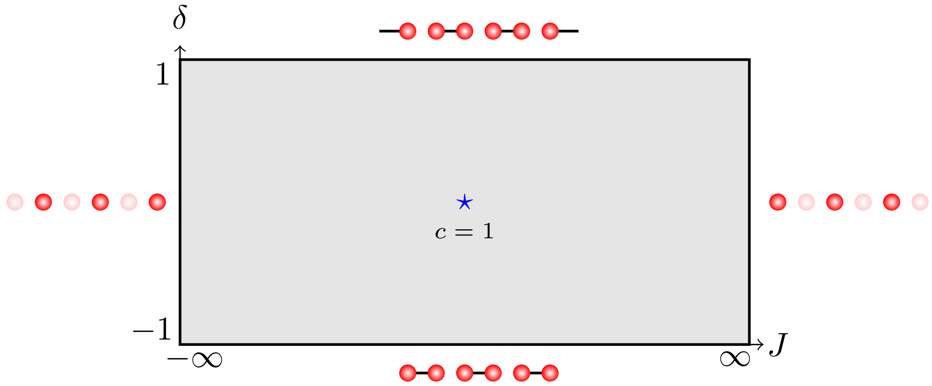

Figure 2.5: Phase diagram of the Rice-Mele model which shows a unit charge getting pumped as we take a parametric path surrounding the gapless point at the origin which is given by a CFT with central charge 1.

the Berry phase in Eqs. (2.8) and (2.9) can be obtained using Stoke's theorem. Let $\bar{\mathcal{M}}_2$ be any two-dimensional surface in the combined parameter and momentum space where the Bloch Hamiltonian does not touch any gap-closing points, whose boundary is purely in the momentum direction corresponding to the Brillouin zone, at some parameter value (J,δ). If we evaluate the integrals in Eqs. (2.13) and (2.14) over $\bar{\mathcal{M}}_2$, after multiplying by a factor of 2π we get, by Stoke's theorem,

$$\gamma(J,\delta) = \int_{\bar{\mathcal{M}}_2} d^2\xi F = \oint_{\partial\bar{\mathcal{M}}_2 = S^1_{\mathrm{BZ}}} A_k(J,\delta)dk. \tag{2.15}$$

In terms of $\hat{g}$, $\gamma(J,\delta)$ can be expressed in terms of the integral in Eq. (2.14) evaluated over $\bar{\mathcal{M}}_2$ and multiplied by a factor of 2π

$$\gamma(J,\delta) = \frac{2\pi}{4\pi}\int_{\bar{\mathcal{M}}_2} d^2\xi \; \hat{g}\cdot(\partial_k\hat{g}\times\partial_\theta\hat{g}) = \frac{1}{2}\int_{\partial\bar{\mathcal{M}}_2 = S^1_{\mathrm{BZ}}} \frac{\hat{g}_x\partial_k\hat{g}_y - \hat{g}_y\partial_k\hat{g}_x}{1+\hat{g}_z}dk. \tag{2.16}$$

This too is another manifestation of Stoke's theorem. Clearly, the choice of $\bar{\mathcal{M}}_2$ is not unique so long as it does not touch any gap closing points. However, the quantization condition in Eq. (2.13) guarantees that a different choice, $\bar{\mathcal{N}}_2$ only shift $\gamma(J,\delta)$ by integer multiples of 2π

$$\int_{\bar{\mathcal{N}}_2} d^2\xi F = \int_{\bar{\mathcal{M}}_2} d^2\xi F - \int_{\bar{\mathcal{M}}_2\cup_{S^1_{\mathrm{BZ}}}\bar{\mathcal{N}}_2} d^2\xi F = \int_{\bar{\mathcal{M}}_2} d^2\xi F - 2\pi \mathsf{C}_1(\bar{\mathcal{M}}_2\cup_{S^1_{\mathrm{BZ}}}\bar{\mathcal{N}}_2) \tag{2.17}$$

where $\bar{\mathcal{M}}_2\cup_{S^1_{\mathrm{BZ}}}\bar{\mathcal{N}}_2$ is the closed manifold obtained by gluing $\bar{\mathcal{M}}_2$ and $\bar{\mathcal{N}}_2$ along their common boundary. We see that the integer shift $\mathsf{C}_1(\bar{\mathcal{M}}_2\cup_{S^1_{\mathrm{BZ}}}\bar{\mathcal{N}}_2)$ depends on whether $\bar{\mathcal{M}}_2\cup_{S^1_{\mathrm{BZ}}}\bar{\mathcal{N}}_2$ encloses any gap-closing loci. In any case, $e^{i\gamma}$ is well-defined, irrespective of the choice of $\bar{\mathcal{M}}_2$.

2.1.2 Estranged edge modes

Protected edge modes are some of the most important features of a topologically non-trivial phase. This has been discussed in [10] as a consequence of the so-called bulk-boundary correspondence. As we have seen, there exists a similar inference that can be made for the case of topological families. We want to now showcase this in the case of the Rice-Mele model. When $\mu = 0$, we have edge modes along the $J = 0,\ \delta \geq 0$ subspace of the phase diagram, owing to the SPT nature of the SSH model that Rice-Mele reduces to along this parameter regime. To show that the edge modes are attributed to the *topological family* and not the SPT nature of the SSH region, we introduce $\mu \neq 0$, breaking the particle-hole symmetry, consequently removing the accidental SPT.

To solve for the edge modes in this case, let us consider the following first-quantized Hamiltonian in real space,

$$\mathrm{h}_{jk} = \left(\delta_{j,k-1}\frac{(1+(-1)^j\delta)}{2}\right) + \left(\delta_{j,k+1}\frac{(1+(-1)^k\delta)}{2}\right) + (J(-1)^j + \mu)\delta_{jk} \tag{2.18}$$

and solve for zero energy eigenstates, $\mathrm{h} \cdot \alpha = 0$. Considering a half-infinite chain, we can isolate zero modes at the left or right boundaries. For $\delta > 0$ and $J = -\mu$ we have a normalisable zero-mode at the left edge with wavefunction

$$\alpha_-(2m+1) \propto \left(\frac{\delta - 1}{\delta + 1}\right)^m . \tag{2.19}$$

For $J = \mu$, the inverted wavefunction gives rise to a zero energy edge mode on the right edge.

The length of localization for the edge modes is given by $\xi \propto 1/\left(\log\left(\frac{1-\delta}{1+\delta}\right)\right)$. For $\delta = 1$, we have $\xi \to 0$ and the localization is over a single lattice point. As we approach the diabolical point $\delta \to 0$, we have $\xi \to \infty$ and the zero modes merge with bulk states as the whole system becomes gapless. Finally, as $\mu \to 0$, we get back the SPT edge modes of the SSH model as the loci of the left and right edge modes merge.

2.2 2d Rice-Mele ascendant

By using the suspension recipe detailed in Chapter D, we hope to explicitly construct a 2d (and higher) ascendant to the Rice-Mele model. Concisely, this procedure is as follows: by stacking a topologically non-trivial system and its inverse along a new spatial direction, and deforming each alternating pair to a trivial one (where a new deformation parameter is introduced), we obtain a higher dimensional topologically non-trivial family. For this, we require to know the form of the inverse of the original Rice-Mele model (consider $\mu = 0$) in the context of the abelian group of phases/Hamiltonians mentioned in Section 1.3. Turns out this is just

$$\mathrm{H}^{inv}_{\mathrm{RM}} = -\mathrm{H}_{\mathrm{RM}} \tag{2.20}$$

One can verify this by noting that $\mathrm{H}^{inv}_{RM} \oplus \mathrm{H}_{RM}$ can be continuously deformed to the trivial family of Hamiltonians without encountering a gap closure.

$$\mathrm{H}_0 = \sum_{x\in\mathbb{Z}} c_1^\dagger(x)c_2(x) + h.c \tag{2.21}$$

Note that our choice of the trivial family is made so that the resultant ascendant is simple. Any other choice can be shown to be smoothly deformed to this family. Let

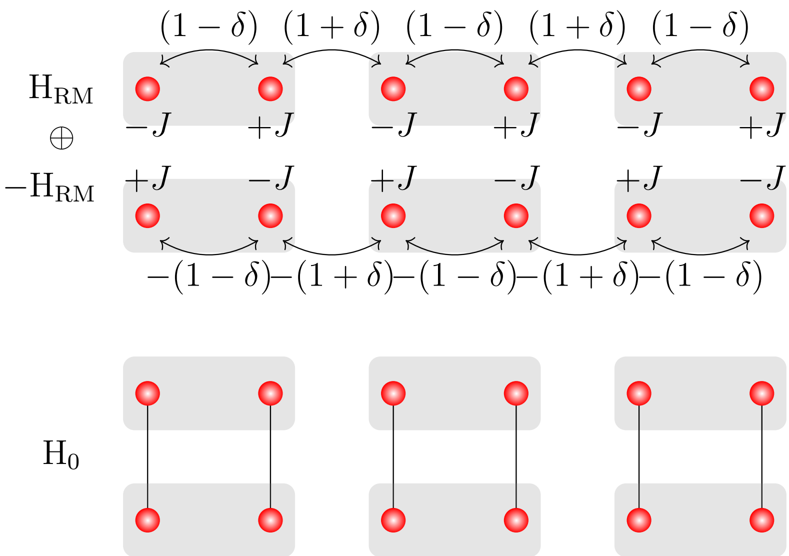

Figure 2.6: H_{RM} stacked with its inverse $-\mathrm{H}_{\mathrm{RM}}$ for $\mu = 0$ and the trivial Hamiltonian family H_0 to which it can be deformed.

us now perform the suspension construction for the Rice-Mele model. Denoting x_1 to be original dimension of the one-dimensional spin chain, we define x_2 to be the new coordinate where we place spin chains which follow H_{RM} and H^{inv}_{RM} alternatively. We further add a hopping anisotropy in this direction called δ_2 as a way of coupling the chains. The Hamiltonian is then given by

$$\mathrm{H}^{[2]}_{\mathrm{RM}}|_{\mu=0} = \sum_{x_2\in\mathbb{Z}} (-1)^{x_2}\mathrm{H}_{\mathrm{RM},x_2}|_{\mu=0} + \sum_{\vec{x}\in\mathbb{Z}^2} \left(\frac{1+(-1)^{x_2}\delta_2}{2}\right)(c^\dagger(\vec{x})c(\vec{x}+\hat{e}_2)+h.c) \tag{2.22}$$

Introducing a chemical potential term for this 2d Hamiltonian, we get:

$$\mathrm{H}^{[2]}_{\mathrm{RM}} = \sum_{\substack{\vec{x}\in\mathbb{Z}^d\\ a=1,2}} t^a_{\vec{x}}\; c^\dagger(\vec{x})c(\vec{x}+\hat{e}_a) + h.c. + \sum_{\vec{x}\in\mathbb{Z}^d} \mu_{\vec{x}} n(\vec{x}) \tag{2.23}$$

where

$$t^1_{\vec{x}} = (-1)^{x_2}\left(\frac{1+(-1)^{x_1}\delta_1}{2}\right),\ t^2_{\vec{x}} = \left(\frac{1+(-1)^{x_2}\delta_2}{2}\right),\ \mu_{\vec{x}} = \mu + (-1)^{x_1+x_2}J\ . \quad (2.24)$$

First, we consider $\mu = 0$. By taking a four-site fiducial unit cell, we can construct the Bloch Hamiltonian to be

$$\mathrm{h}(\vec{k}) = \mu\mathbb{1} + \sum_{m=1}^{5} g_m(\vec{k})\Gamma^m \quad (2.25)$$

where, corresponding to a particular choice of the unit cell and correspondingly the spinor, ψ, we have

$$\begin{aligned} g_1 &= \frac{(1-\delta_1)}{2} + \frac{(1+\delta_1)}{2}\cos(k_1),\ g_2 = \frac{(1+\delta_1)}{2}\sin(k_1), \\ g_3 &= \frac{(1-\delta_2)}{2} + \frac{(1+\delta_2)}{2}\cos(k_2),\ g_4 = \frac{(1+\delta_2)}{2}\sin(k_2), \\ g_5 &= J. \end{aligned} \quad (2.26)$$

The $\{\Gamma^\mu\}$, are elements of the irreducible representation of the Clifford algebra $Cl(5)$, satisfying

$$\{\Gamma^m, \Gamma^n\} = 2\delta_{mn}. \quad (2.27)$$

The matrix representation of $\{\Gamma^\mu\}$ for our current choice of unit cell is

$$\begin{aligned} &\Gamma_1 = \sigma^3 \otimes \sigma^1,\ \Gamma_2 = \sigma^3 \otimes \sigma^2,\ \Gamma_3 = \sigma^1 \otimes \mathbb{1}, \\ &\Gamma_4 = \sigma^2 \otimes \mathbb{1}, \Gamma_5 = \sigma^3 \otimes \sigma^3. \end{aligned} \quad (2.28)$$

Probing the energy dispersion for this model for different values of the parameters $\delta_1,\ \delta_2 \in [-1, 1],\ J \in (-\infty, \infty)$, we find that the theory is gapless, resulting in a Dirac point, at $J = \delta_1 = \delta_2 = 0$, and is gapped everywhere else on the parameter space. This can be seen in Fig. 2.7.

2.2.1 Topological features

From the suspension construction motivated by Kitaev's proposal, one would expect that the family of states surrounding the gapless point at $\delta_1 = \delta_2 = J = 0$ to be topologically non-trivial over $\Sigma S^1 = S^2$. This can be encapsulated by computing the second Chern number. We have two entirely filled bands $|\varepsilon^-_{1,2}\rangle$ in this four band model at zero chemical potential. Consider the (non-abelian) Berry connection defined as follows

$$[A_\mu(\xi)]_{ab} = -i\langle\varepsilon^-_a(\xi)|\frac{\partial}{\partial\xi_\mu}|\varepsilon^-_b(\xi)\rangle \quad (2.29)$$

where ξ_μ denote the collective coordinates taking values in both the Brillouin zone (the momenta) and the parameter space. Now, take the family of states on a sphere

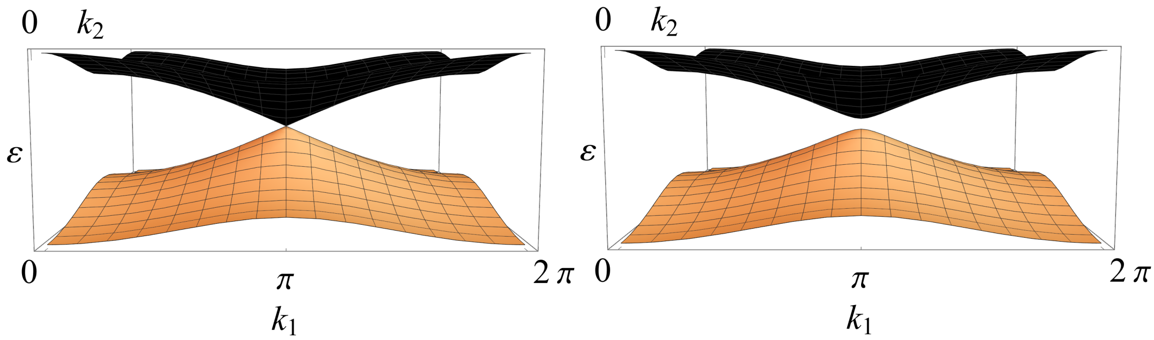

(a) $\delta_1 = \delta_2 = J = 0$ (b) Away from the origin

Figure 2.7: Band dispersions for the 2d ascendant of the Rice-Mele model.

surrounding the origin. Define $\mathcal{M}_4 = S^2_{par} \times T^2_{BZ}$. One can compute the second Chern number by an integral over the non-abelian Berry connection as follows [29, 30, 31, 32, 33, 22, 21]:

$$\mathsf{C}_2(\mathcal{M}_4) = \frac{1}{32\pi^2} \int_{\mathcal{M}_4} d^4\xi \; \epsilon^{\mu\nu\alpha\beta} \, \mathrm{tr}(F_{\mu\nu} F_{\alpha\beta}) \tag{2.30}$$

where, $F_{\mu\nu}$ is the non-abelian Berry curvature,

$$F_{\mu\nu} = \partial_\mu A_\nu - \partial_\nu A_\mu + [A_\mu, A_\nu] \tag{2.31}$$

One can verify that C_2 in fact turns out to be 1. Check Chapter C for more details on the numerical results and graphs. For the case of non-interacting models, Eq. (2.30) can be given a nice expression in terms of $\hat{g}_m = g_m/|g|$, as

$$\mathsf{C}_2(\mathcal{M}_4) = \frac{3}{8\pi^2} \int_{\mathcal{M}_4} d^4\xi \epsilon_{abcde} \epsilon^{\mu\nu\alpha\beta} \hat{g}^a \partial_\mu \hat{g}^b \partial_\nu \hat{g}^c \partial_\alpha \hat{g}^d \partial_\beta \hat{g}^e \tag{2.32}$$

where $\hat{g}$ now defines a map $\hat{g} : \mathcal{M}_4 \to S^4$ and $\mathsf{C}_2(\mathcal{M}_4)$ defined as here counts the degree of winding of this map.

For the purpose of the texture in this case, we claim that the analogous geometric invariant to the Berry phase can be defined as the higher Berry phase through Stokes' theorem from the second Chern number. Consider evaluating Eq. (2.30) over a 4-manifold with a boundary $\bar{\mathcal{M}}_4$, $\partial\bar{\mathcal{M}}_4 = \mathcal{M}_3 = T^2_{\mathrm{BZ}} \times S^1_{\mathrm{par}}$, where S^1_{par} is some circle in parameter space where there is no gap closure. Multiplying this by a factor of 2π, we get

$$\begin{aligned}\check{\gamma}(S^1_{\mathrm{par}}) &= \frac{1}{16\pi} \int_{\bar{\mathcal{M}}_4} d^4\xi \; \epsilon^{\mu\nu\alpha\beta} \, \mathrm{tr}(F_{\mu\nu} F_{\alpha\beta}) \\ &= \frac{1}{4\pi} \int_{\mathcal{M}_3} d^3\xi \; \epsilon^{\mu\nu\alpha} \, \mathrm{tr}\left(A_\mu \partial_\nu A_\alpha + \frac{2}{3} A_\mu A_\nu A_\alpha \right) .\end{aligned} \tag{2.33}$$

Eq. (2.33) is an integral of the Chern-Simons form CS_3 which assigns an unquantized $U(1)$ geometric invariant for every circle (more generally a closed one-dimensional loop) in parameter space that does not depend on the choice of $\bar{\mathcal{M}}_4$. To see this, consider two bounding 4-manifolds $\bar{\mathcal{M}}_4$ and $\bar{\mathcal{N}}_4$ with the same boundary $\partial\bar{\mathcal{M}}_4 = \partial\bar{\mathcal{N}}_4 = \mathcal{M}_3 = T^2_{\mathrm{BZ}} \times S^1_{\mathrm{par}}$. We then have

$$\frac{1}{16\pi}\int_{\bar{\mathcal{N}}_4} d^4\xi\ \epsilon^{\mu\nu\alpha\beta}\,\mathrm{tr}(F_{\mu\nu}F_{\alpha\beta}) = \frac{1}{16\pi}\int_{\bar{\mathcal{M}}_4} d^4\xi\ \epsilon^{\mu\nu\alpha\beta}\,\mathrm{tr}(F_{\mu\nu}F_{\alpha\beta}) - 2\pi\mathsf{C}_2(\bar{\mathcal{M}}_4 \cup_{\bar{\mathcal{M}}_3} \mathcal{N}_4). \quad (2.34)$$

$\bar{\mathcal{M}}_4 \cup_{\mathcal{M}_3} \bar{\mathcal{N}}_4$ is a 4-manifold without any boundaries that is obtained by gluing $\bar{\mathcal{M}}_4$ and $\bar{\mathcal{N}}_4$ along their common boundary. The multiplicative factor of 2π compared to Eq. (2.30) allows $\check{\gamma}$ to be restricted to the fundamental domain, $\check{\gamma} \in [0, 2\pi]$ making $e^{i\check{\gamma}}$ a well-defined phase for any choice of $\bar{\mathcal{M}}_4$ and depend only on the boundary $\mathcal{M}_3 = S^1_{\mathrm{par}} \times T^2_{\mathrm{BZ}}$ and ultimately only on S^1_{par}. Eq. (2.33) can also be evaluated using a modification of the expression in Eq. (2.32):

$$\check{\gamma}(S^1_{\mathrm{par}}) = \frac{3}{4\pi}\int_{\bar{\mathcal{M}}_4} d^4\xi\epsilon_{abcde}\epsilon^{\mu\nu\alpha\beta}\hat{g}^a\partial_\mu\hat{g}^b\partial_\nu\hat{g}^c\partial_\alpha\hat{g}^d\partial_\beta\hat{g}^e \quad (2.35)$$

Indeed, Berry's phase in Eq. (2.8) can be interpreted as an integral over Chern-

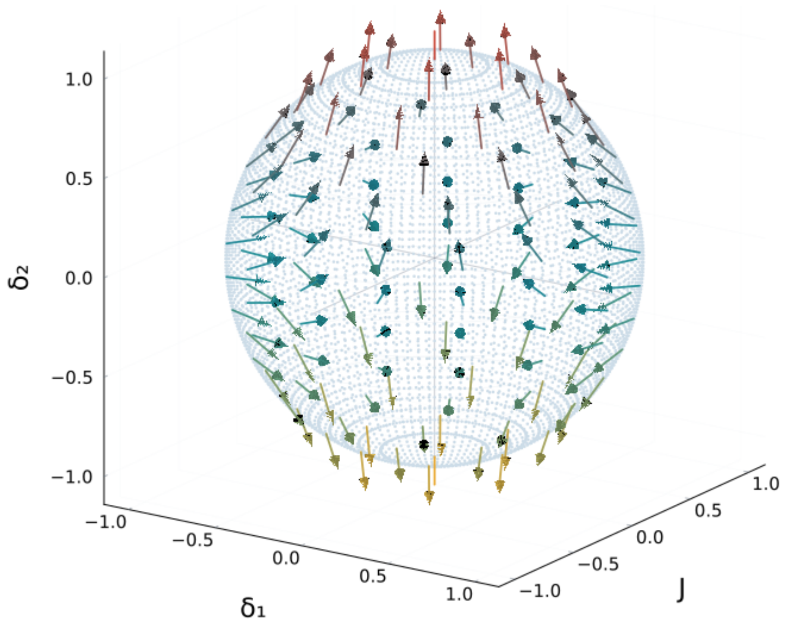

Figure 2.8: Topological texture for the 2d ascendant of the Rice-Mele model on the sphere obtained by plotting the $U(1)$ higher Berry invariant along each latitude.

Simons form CS_1, making the expression in Eq. (2.33) a natural generalization as well as higher dimensional extensions.

To visualize this on the phase diagram, we compute the geometric invariant for every latitude on the parameter space, integrating over all the other parameters. This gives us a $U(1)$ quantity. We now make a heuristic choice of inferring this as the angle formed by a vector in the tangent-normal plane for each point on the latitude of the sphere with respect to the tangent. This can be seen in Fig. 2.8.

2.3 Edge modes

To study the edge modes in this case, we take open boundary conditions in the x_2 direction. We visualize this in Fig. 2.9(a). This introduces two disjoint open edges.

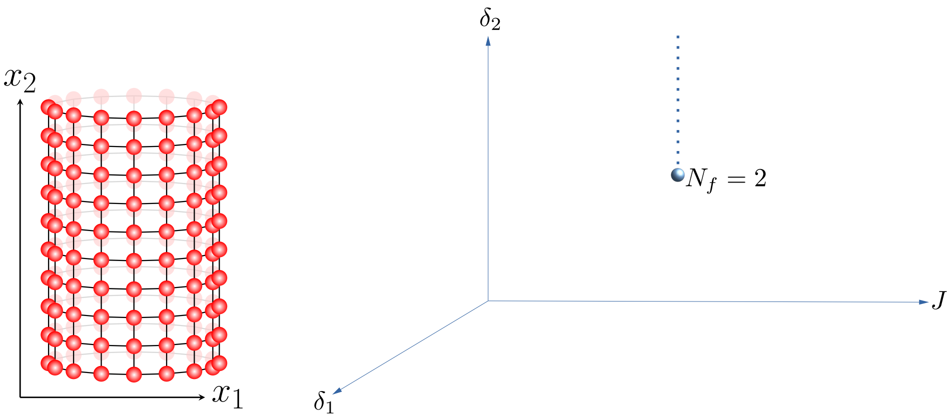

(a) (b) $\mu = 0$

Figure 2.9: Left: schematic of the 2d lattice with open boundary in the x_2 direction. Right: Phase diagram for $\mu = 0$.

The loci of the edge modes can be understood intuitively in the limit $\delta_2 = 1$ as follows: the open edges are reminiscent of a 1d Thouless pump. Then this problem basically reduces to asking when this chain is gapless in the bulk. As we have seen in Section 2.1, this happens when $\delta_1 = J = 0$. On this account, we have plotted the locus of the edge modes on the phase diagram in Fig. 2.9(b). Now we tune $\mu \neq 0$. We first note that the 2d bulk becomes gapless for the parameter regions enclosed by the sphere $J^2 + \delta_1^2 + \delta_2^2 = \mu^2$. Utilizing the same intuition for when $\delta_2 = 1$, we can state that the new locus of zero energy edge modes would be when $\delta_1^2 + J^2 \leq \mu^2$. We finally note that these results have been verified numerically and the full picture can be seen in Fig. 2.10.

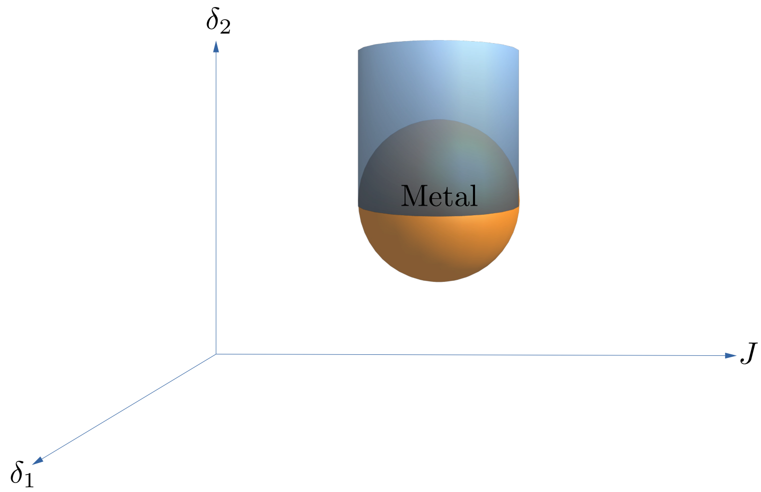

Figure 2.10: Phase diagram for $\mu > 0$ and $|\mu| < 1$. The parameter region where edge modes appear while is denoted in blue. The edge modes terminate on the spherical region at the origin representing a metal with partially filled bands.

2.4 Field theory analysis

We now want to verify the stability of the topological features using field theoretic techniques. Consider $\mu = 0$. By performing a small wavelength expansion about the points (π, π) in the Brillouin zone, $\vec{g}$ becomes

$$g_1 = -\delta_1,\ g_2 = vq_1,\ g_3 = -\delta_2,\ g_4 = vq_2,\ g_5 = J \tag{2.36}$$

where we omit the v in the field theoretic Hamiltonian:

$$\mathrm{H} \approx \int d^2x\ \psi^\dagger(\vec{x})\Big(i\Gamma_2\partial_{x_1} + i\Gamma_4\partial_{x_2} - \delta_1\Gamma_1 - \delta_2\Gamma_3 + J\Gamma_5\Big)\psi(\vec{x}) \tag{2.37}$$

where ψ is a 4-component ($N_f = 2$) Dirac spinor. One can write this in terms of the Lagrangian density in terms of the two flavours of irreducible two-component Dirac spinors. For this, we choose the basis decomposition as follows

$$\begin{aligned}&\gamma_0 = \sigma^1 \otimes \sigma^2, \gamma_1 = -\sigma^2 \otimes \mathbb{1}, \gamma_2 = \sigma^3 \otimes \sigma^2,\\ &\tau^1 = \sigma^2 \otimes \sigma^3, \tau^2 = \mathbb{1} \otimes \sigma^2, \tau^3 = -\sigma^2 \otimes \sigma^1.\end{aligned} \tag{2.38}$$

Here, γ_μ and τ_μ are 4×4 matrices each following the $(2+1)$d mutually commuting Clifford algebras which is easy to verify. One can further check that this basis choice preserves the algebra of the Γ_μ (here, μ runs from 1 to 5) matrices, which it should. The Lagrangian density can now be obtained by

$$\mathcal{L} = i\psi^\dagger\partial_t\psi - \mathcal{H} \tag{2.39}$$

$$\mathcal{L} = -\sum_{a=1}^{2}\bar{\psi}_a\partial\!\!\!/\psi_a - \sum_{a,b=1}^{2}\bar{\psi}_a\left(\vec{m}.\vec{\tau}_{ab}\right)\psi_b. \tag{2.40}$$

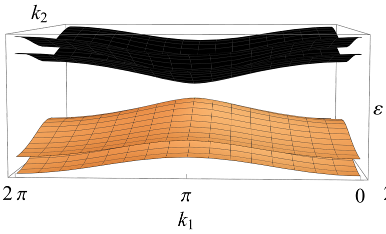

(a) $J = \delta_1 = \delta_2 = 0$

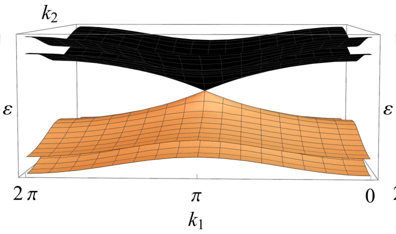

(b) $J^2 + \delta_1^2 + \delta_2^2 = m_s^2$

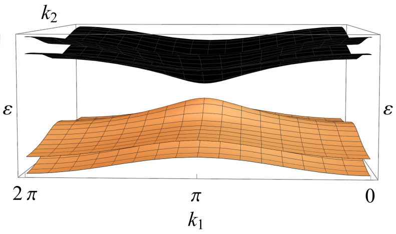

(c) $J^2 + \delta_1^2 + \delta_2^2 > m_s^2$

Figure 2.11: Band dispersion plots after we add a singlet mass term with coefficient m_s. At (a) we have gapped out the $N_f = 2$ Dirac fermion we had prior to adding the mass term while at (b) we have a single flavour Dirac fermion. As we move away, (c) we again gap the bands out.

where, we have defined

$$\vec{m} = (\delta_1, \delta_2, J) \tag{2.41}$$

Eq. (2.40) represents a two-flavor Dirac fermion perturbed by the "triplet" mass terms as given. It is known that an additional relevant singlet mass with the same scaling dimensions of the form $m_s \sum_a \bar{\psi}_a \psi_a$ could be added. However, it turns out that the triplet and singlet mass terms are not fully independent. The effect on the dispersion of adding such a term to our Hamiltonian can be seen in Fig. 2.11.

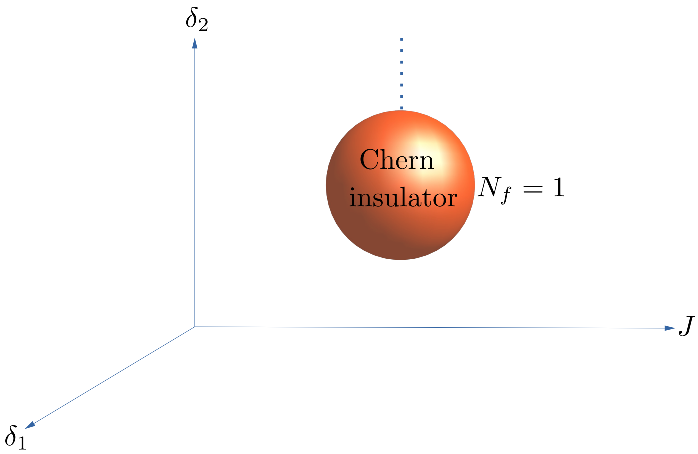

Figure 2.12: The phase diagram after the addition of the singlet mass m_s.

At the single-particle level, while all four mass matrices anti-commute with the gamma matrices of the kinetic term, the singlet mass commutes with all triplet masses and can be simultaneously diagonalized. Thus, the space of *independent* relevant masses is three-dimensional. For $|m_s| < 1$ and $\mu = 0$, this results in two filled, non-degenrate bands but one of them (the one closest to the Fermi level) carries non-zero Chern number, resulting in a Chern insulating state as shown in Fig. 2.12. The opposite Chern number is carried by one of the unoccupied bands closest to the Fermi level. As we radially increase δ_1, δ_2, J, the two Chern bands again meet along the sphere $\delta_1^2 + \delta_2^2 + J^2 = m_s^2$ resulting in a gapless single-flavor $N_f = 1$ massless Dirac theory and open again reproducing the trivial phase with the texture as shown in Fig. 2.11.

This remarkably means that all the relevant perturbations of the Dirac point are already present in the model and any other $U(1)$-preserving terms will in turn keep the Dirac point. One can argue that the presence of the gapless diabolical point is what sources the non-trivial topology of the family surrounding it. This has been alluded to in Section 1.3.1. Hence, the topological features elucidated previously turn out to be absolutely stable on addition of any $U(1)$-preserving terms to the Hamiltonian.

2.5 Rice-Mele ascendants in arbitrary dimensions

Using methods discussed in Chapter D, we construct $(d+1)-$dimensional ascendants for the Rice-Mele model formed using those in $d-$dimensions. This gives us

$$\mathrm{H}_{\mathrm{RM}}^{[d]} = \mu \sum_{\vec{x}\in\mathbb{Z}^d} n(\vec{x}) + \sum_{x_d\in\mathbb{Z}} (-1)^{x_d} \mathrm{H}_{\mathrm{RM},x_d}^{[d-1]}|_{\mu=0} + \sum_{\vec{x}\in\mathbb{Z}^d} \left(\frac{1+(-1)^{x_d}\delta_d}{2}\right) (c^\dagger(\vec{x})c(\vec{x}+\hat{e}_d) + h.c) \tag{2.42}$$

The iterated, expanded form similar to Eq. (2.23) can also be determined

$$\mathrm{H}_{\mathrm{RM}}^{[d]} = \sum_{\substack{\vec{x}\in\mathbb{Z}^d \\ a=1\ldots d}} t_{\vec{x}}^a \, c^\dagger(\vec{x})c(\vec{x}+\hat{e}_a) + h.c. + \sum_{\vec{x}\in\mathbb{Z}^d} \mu_{\vec{x}} n(\vec{x}) \tag{2.43}$$

where, the staggered hopping amplitudes $t_{\vec{x}}^a$ for $a = 1, \ldots, d$ and chemical potential $\mu_{\vec{x}}$ are defined as

$$\begin{aligned} t_{\vec{x}}^a &= (-1)^{\sum_{k=a}^d x_k} \left(\frac{1+(-1)^{x_a}\delta_a}{2}\right), \\ \mu_{\vec{x}} &= \mu + (-1)^{\sum_{k=1}^d x_k} J. \end{aligned} \tag{2.44}$$

For this, one can define a 2^d band Hamiltonian as follows:

$$\mathrm{h}(\vec{k}) = \mu\mathbb{1} + \sum_{m=1}^{2d+1} g_m(\vec{k})\Gamma^m \ , \tag{2.45}$$

where, for a particular choice of unit cell, we have

$$
\begin{aligned}
g_{2m-1}(\vec{k}) &= \frac{(1-\delta_m)}{2} + \frac{(1+\delta_m)}{2}\cos(k_m),\\
g_{2m}(\vec{k}) &= \frac{(1+\delta_m)}{2}\sin(k_m),\ m = 1,\dots,d,\\
g_{2d+1}(\vec{k}) &= (-1)^d J\ .
\end{aligned} \tag{2.46}
$$

The $\{\Gamma^m\}$ represent the d dimensional irrep of the Clifford algebra $Cl(2d+1)$ satisfying Eq. (2.27) whose matrix representation for the same unit cell choice is given by

$$
\begin{aligned}
\Gamma^{2m+1} &= \underbrace{\sigma^3\otimes\sigma^3\cdots\otimes\sigma^3}_{\text{d-m terms}}\otimes\sigma^1\otimes\underbrace{\mathbb{1}\otimes\mathbb{1}\otimes\cdots\otimes\mathbb{1}}_{\text{m-1 terms}}\\
\Gamma^{2m} &= \underbrace{\sigma^3\otimes\sigma^3\cdots\otimes\sigma^3}_{\text{d-m terms}}\otimes\sigma^2\otimes\underbrace{\mathbb{1}\otimes\mathbb{1}\otimes\cdots\otimes\mathbb{1}}_{\text{m-1 terms}}\\
\Gamma^{2d+1} &= \underbrace{\sigma^3\otimes\sigma^3\cdots\otimes\sigma^3}_{\text{d terms}},\ m = 1,\dots,d
\end{aligned} \tag{2.47}
$$

The model has two bands each of which is 2^{d-1} fold degenerate with eigenvalues

$$
\varepsilon_\pm(\vec{k}) = \mu \pm |g(\vec{k})|,\ |g(\vec{k})| = \sqrt{\sum_{m=1}^{2d+1}|g_m(\vec{k})|^2} \tag{2.48}
$$

To probe the topological non-triviality of the model, we define C_d

$$
\mathsf{C}_d = \frac{1}{d!}\int_{\mathcal{M}_{2d}} \mathrm{tr}\left(\overbrace{\frac{F}{2\pi}\wedge\frac{F}{2\pi}\wedge\cdots\wedge\frac{F}{2\pi}}^{\text{d terms}}\right) \tag{2.49}
$$

The expression for Eq. (2.49) reduces to the calculation of the winding of the map $\hat{g}$

$$
\mathsf{C}_d = \frac{\epsilon^{a_1a_2\cdots a_{2d+1}}}{\mathcal{V}(S^{2d})}\int_{\mathcal{M}_{2d}} \hat{g}_{a_1}\wedge d\hat{g}_{a_2}\cdots\wedge d\hat{g}_{a_{2d+1}}. \tag{2.50}
$$

where, $\mathcal{V}(S^k)$ denotes the volume of the k unit sphere given by the formula

$$
\mathcal{V}(S^k) = \frac{2\pi^{k/2}}{\Gamma\left(k/2\right)} \tag{2.51}
$$

The non-trivial nature of the family of states can also be determined through a topological texture visible by studying a geometric invariant, $\check{\gamma}$. This is defined for any closed $d-1$ dimensional surface, such as S^{d-1} on the parameter space. Let

$\mathcal{M}_{2d-1} = S^{d-1} \times T^d_{\mathrm{BZ}}$ and let $\bar{\mathcal{M}}_{2d}$ be a manifold such that its boundary contains $\mathcal{M}_{2d-1}$ i.e., $\partial\bar{\mathcal{M}}_{2d} = \mathcal{M}_{2d-1}$. $\check{\gamma}$ is defined using the integral in Eq. (2.49) evaluated on $\bar{\mathcal{M}}_{2d}$ as

$$\check{\gamma} = \frac{2\pi}{d!}\int_{\bar{\mathcal{M}}_{2d}} \mathrm{tr}\left(\overbrace{\frac{F}{2\pi} \wedge \frac{F}{2\pi} \wedge \cdots \wedge \frac{F}{2\pi}}^{\text{d terms}}\right) = \int_{\mathcal{M}_{2d-1}} \mathsf{CS}_{2d-1} \tag{2.52}$$

where, we have used Stoke's theorem to rewrite $\check{\gamma}$ as an integral over the Chern-Simons form CS_{2d-1}. The exact expressions for CS_{2d-1} varies with d. We have already encountered the form for $d = 1, 2$. For $d = 3$, we have

$$\mathsf{CS}_5 = \frac{1}{3!}\frac{1}{(2\pi)^3}\,\mathrm{tr}\Big(A \wedge F \wedge F + \frac{3}{2}A \wedge A \wedge A \wedge F + \frac{3}{5}A \wedge A \wedge A \wedge A \wedge A\Big). \tag{2.53}$$

Written in terms of $\hat{g}$, the expression for $\check{\gamma}$ reduces to

$$\check{\gamma} = \frac{2\pi}{\mathcal{V}(S^{2d})}\int_{\bar{\mathcal{M}}_{2d}} \epsilon^{a_1 a_2 \cdots a_{2d+1}} \hat{g}_{a_1} \wedge d\hat{g}_{a_2} \cdots \wedge d\hat{g}_{a_{2d+1}}. \tag{2.54}$$

Although direct visualization in higher dimensions is not possible, the higher Berry phases evaluated using Eqs. (2.52) and (2.54) can be used to reveal the topological textures present in the phase diagrams following strategies analogous to the ones used in one and two spatial dimensions.

2.6 Berry's model

We now move onto the second series of topologically non-trivial families that can be constructed sequentially using the suspension construction. The first member of this is the familiar spin in a magnetic field as described in Section 1.3.1. To put this in the current context, one can plot the $U(1)$ Berry phase for each latitude as we had done for the higher Berry phase in the case of the 2d Rice-Mele ascendant. This is done in Fig. 2.13.

2.7 Higher ascendants of Berry's model

By using the suspension construction, we can construct higher ascendants of Berry's model. First, however, we fermionize the original Berry model to obtain

$$\mathrm{H}_{\mathrm{Berry}} = \sum_{\alpha,\beta\in\{\uparrow,\downarrow\}} c^\dagger_\alpha(\vec{B}.\vec{\sigma}_{\alpha\beta})c_\beta + \mu \sum_{\alpha\in\{\uparrow,\downarrow\}} c^\dagger_\alpha c_\alpha \tag{2.55}$$

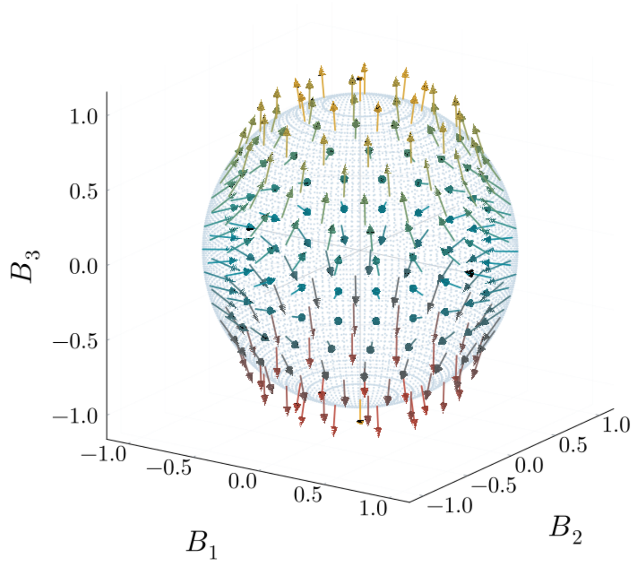

Figure 2.13: Texture on S^2 for the Berry's model of a spin in a magnetic field which is plotted by computing the Berry phase for each latitude.

where the first quantized Hamiltonian is the quantum-mechanical spin in a magnetic field (for $\mu = 0$). Now, we can construct the 1-dimensional ascendant of the same:

$$\mathrm{H}_1(\hat{n}_{S^3}) = \sum_{x\in\mathbb{Z}}(-1)^x \mathrm{H}_{0x}(n_1,n_2,n_3) + \sum_{x\in\mathbb{Z}} \frac{(1+(-1)^x n_4)}{2} \sum_{\alpha\in\uparrow,\downarrow} \left(c^\dagger_\alpha(x)c_\alpha(x+1) + h.c.\right). \tag{2.56}$$

Here, $\hat{n} = \{n_1, n_2, n_3, n_4\}$, denoting a 4-component unit vector parametrizing S^3. Also, H_0 is just the topologically non-trivial family as in Eq. (2.55). This model has a two-site fiducial unit cell, and therefore, we get the following four-band model (two spinor indices denoting the spin and two for the sites in the unit cell),

$$\mathrm{H}_1(\hat{n}_{S^3}) = \sum_k \psi^\dagger(k)\mathrm{h}_1(\hat{n}_{S^3},k)\psi(k), \tag{2.57}$$

$$\mathrm{h}_1(\hat{n}_{S^3},k) = g_a(\hat{n}_{S^3},k)\Gamma^a. \tag{2.58}$$

where,

$$g_1 = n_1,\ g_2 = n_2,\ g_3 = n_3,\ g_4 = \frac{(1-n_4)}{2} + \frac{(1+n_4)}{2}\cos k,\ g_5 = \frac{(1+n_4)}{2}\sin k. \tag{2.59}$$

and

$$\Gamma_1 = -\sigma^3 \otimes \sigma^1,\ \Gamma_2 = -\sigma^3 \otimes \sigma^2,\ \Gamma_3 = -\sigma^3 \otimes \sigma^3,$$
$$\Gamma_4 = \sigma^1 \otimes \mathbb{1},\ \Gamma_5 = \sigma^2 \otimes \mathbb{1}. \tag{2.60}$$

The states can be verified to be gapped for all values of $\hat{n} \in S^3$. The single-particle energies of the first-quantized Hamiltonian in Eq. (2.58) can be determined as $\pm\varepsilon(\hat{n}, k)$

$$\mathrm{h}_1^2(\hat{n}, k) = \varepsilon^{\pm}(\hat{n}, k)\mathbb{1} \tag{2.61}$$
$$\varepsilon^{\pm}(\hat{n}, k) = \pm\sqrt{g_a(\hat{n}, k)g^a(\hat{n}, k)} \tag{2.62}$$

To note that the family of states parametrized on S^3 is in fact non-trivial, we construct the non-abelian Berry connection,

$$[A_\mu]_{ab} = -i\langle\varepsilon_a^-|\frac{\partial}{\partial\xi_\mu}|\varepsilon_b^-\rangle \tag{2.63}$$

where $\xi_\mu,\ \mu = 1, \ldots, 4$ are collective coordinates for the parametric S^3 as well as the momentum in the Brillouin zone i.e. for the 4-manifold, $\mathcal{M}_4 = S^3 \times S^1$. The structure of the Berry connection is given by the group $U(2)$. Note that the non-vanishing of the trace is related to the fact that the eigenstate degeneracy for each eigenstate is 2. The second Chern number and the higher Berry phase can be computed respectively using the sets of equations Eq. (2.30), Eq. (2.32), Eq. (2.33) and Eq. (2.35).

One can by analogy build higher dimensional generalizations,

$$\begin{aligned}\mathrm{H}_d(\hat{n}_{S^{d+2}}) = &\sum_{x_d \in \mathbb{Z}} (-1)^{x_d} \mathrm{H}_{d-1,x_d}(n_1, n_2, n_3, \ldots, n_{d+2}) \\ &+ \sum_{x_d \in \mathbb{Z}} \frac{(1 + (-1)^{x_d} n_{d+3})}{2} \sum_{\alpha \in \uparrow,\downarrow} \left(c_\alpha^\dagger(\vec{x})c_\alpha(\vec{x} + \hat{e}_d) + h.c.\right)\end{aligned} \tag{2.64}$$

with associated higher Chern numbers acting as respective diagnoses of topological non-triviality.

Chapter 3

Topological Metals

We will relax one of the properties of the topological phases appearing in the previous chapters: we allow the bulk to now be gapless. In this subclass, there appear to be a wide slew of experimentally realizable materials with exciting transport properties. We will briefly describe some landmark examples of the same before we move onto some original work including working towards a novel topological invariant.

3.1 Weyl semi-metal

The first of these topological semi-metals is obtained by having two Weyl points in the Brillouin zone. One can expect these to source some non-trivial topology by noticing that Weyl points serve as Berry curvature monopoles [34].

Accidental degeneracies

Consider a quantum mechanical system with no symmetries. Generically, one has a large set of eigenvalues to consider. But our current objective is to look at conditions for two energy levels to be made degenerate with respect to a parameter λ. Reducing to these energy levels, one can write any 2×2 Hamiltonian using the Pauli matrices:

$$\mathrm{H}_{12} = f_0 \mathbb{1} + f_x(\lambda)\sigma^1 + f_y(\lambda)\sigma^2 + f_z(\lambda)\sigma^3 \tag{3.1}$$

For the energy gap to vanish, we need to separately tune $f_x = f_y = f_z = 0$. For this to have a solution, we generically need to tune 3 parameters.

Inversion symmetric model

To have 3 parameters to tune, we look at a model in 3 spatial dimensions. An important part of the previous argument is that we have non-degenerate bands. Usually, having both time-reversal and inversion symmetries enforce a degeneracy ($T^2 = -1$ for 3D fermions):

$$\mathrm{H}(\vec{k}) \longrightarrow \mathcal{U}_T \mathrm{H}(-\vec{k}) \mathcal{U}_T^\dagger \longrightarrow \mathcal{U}_{IT} \mathrm{H}(\vec{k}) \mathcal{U}_{IT}^\dagger \tag{3.2}$$

since we don't want this, we have to either break T or I. For this reason, we look at a model with broken time-reversal symmetry but preserving inversion. There is a certain assignment of parity eigenvalues to Time Reversal Invariant Momenta (TRIM) for which there's no way the system can be gapped throughout and hence acts as a guarantee that we get gap touching loci. Turns out this actually allows for a case with a minimal set of two Weyl nodes at the same energy. The dispersion relation can be visualised as in

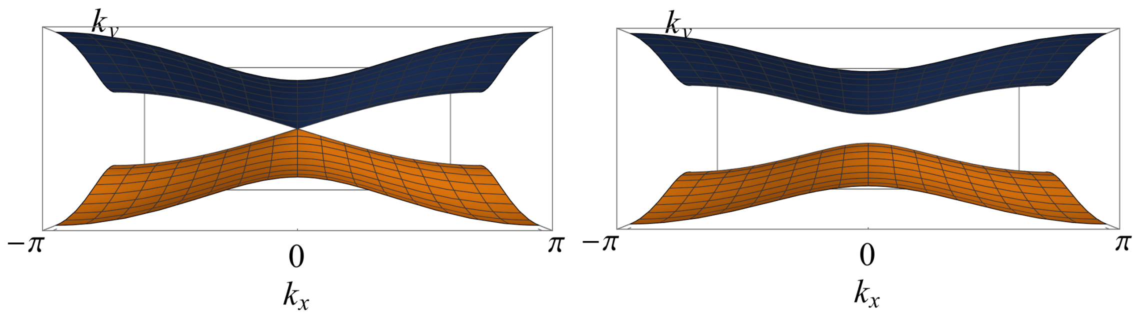

(a) (b)

Figure 3.1: Dispersion relation of the Weyl semi-metal for the parameter values $t = 1,\ \gamma = 0$. (a) showcases the Weyl point at $k_z = \frac{\pi}{2}$ while (b) showcases the slice at $k_z = -\pi$.

$$\mathrm{h}(\vec{k}) = t(2 + \gamma - \cos k_x - \cos k_y - \cos k_z)\tau^z + t \sin k_x \tau^x + t \sin k_y \tau^y \tag{3.3}$$

$$\mathrm{h}(\vec{k}) \longrightarrow \tau^z \mathrm{h}(-\vec{k}) \tau^z \tag{3.4}$$

For $\gamma \in [-1, 1]$, there exist two Weyl points at $(0, 0, \pm k_0)$.

The topological non-triviality in this case can be understood by computing the Chern number for the Hamiltonian family on a manifold surrounding the gapless points. This turns out to give $+1$ and -1 respectively for the nodes. A deeper reason for this is the Nielson-Ninomiya theorem which states that Weyl nodes only occur in pairs with the total charge amounting to zero.

Now, since the system is topological for $\gamma \in [-1, 1]$, we have detectable edge modes. These can be seen by opening up the boundary conditions in the $y-$direction but keeping the periodicity in the other two; so k_x and k_z are valid quantum numbers still.

$$c_{(k_x,k_y,k_z)} = \frac{1}{N_y}\sum_{n=1}^{N} e^{ik_y n} c_{(k_x,k_y),n} \tag{3.5}$$

Calling the $(k_x, k_z) = \vec{k}$, we get the Hamiltonian as,

$$\begin{aligned}\mathrm{H}(\vec{k}) = \frac{t_z}{2}\sum_{n,\alpha,\beta}\tau^z_{\alpha,\beta}(c_{\vec{k},n+1,\alpha}c_{\vec{k},n,\beta} + h.c.) + \frac{t_y}{2}\sum_{n,\alpha,\beta}\tau^y_{\alpha,\beta}(ic_{\vec{k},n+1,\alpha}c_{\vec{k},n,\beta} + h.c.)\\ + t_x\sum_{\vec{k},n}\sin(k_x)\tau^x_{\alpha,\beta}c^\dagger_{\vec{k},n,\alpha}c_{\vec{k},n,\beta} + t_z\sum_{\vec{k},n}(2-\gamma-\cos(k_x)-\cos(k_z))\tau^x_{\alpha,\beta}c^\dagger_{\vec{k},n,\alpha}c_{\vec{k},n,\beta}\end{aligned} \tag{3.6}$$

These edge modes can be visualized as in Fig. 3.2. Their existence can be argued in

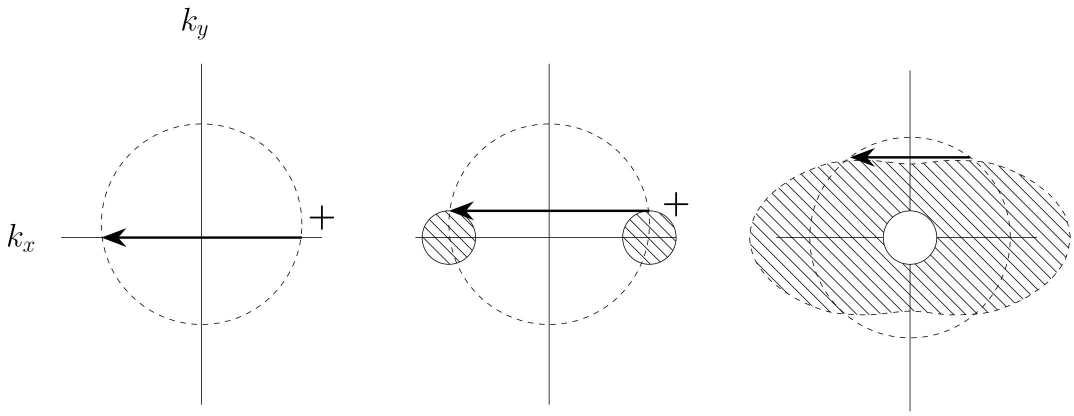

Figure 3.2: The Weyl semi-metal after taking open boundary conditions along the k_Z direction. We see Fermi surface arc states connecting the Weyl points (left) when $\mu = 0$. As we increase the chemical potential, the points get enveloped by charged Fermi surface spheres which still have arc states tangent to them (middle). Further increasing μ, we undergo a Lifshitz transtion changing the Fermi surface topology (right).

two equivalent ways. The first of this involves the fact that in between the two Weyl points, there exist a sheet of topologically non-trivial insulators with $\mathsf{C}_1 = 1$. These in turn harbor edge modes which collectively can be taken to form the Fermi arc states. The second involves a similar anomaly cancellation argument stemming from the IR description near the Weyl points. These "fermions" are known to have a chiral anomaly in (3+1)D; the existence of chiral Fermi arc states rely on the cancellation of this anomaly function.

That these surface states terminate at the Weyl points is a direct consequence of the fact that these a Berry curvature monopoles [34]. Further, it has been argued that these Fermi arcs seep into the bulk at the gapless nodes. For a mathematical perspective on the same, we refer to [35].

Weyl metal

On increasing chemical potential to a finite value, the topology of the Fermi surface changes into being two disconnected spheres enveloping the two nodes. At a certain value of μ, the Fermi surface undergoes a Lifshitz transition and we cease to call this a Weyl metal phase. Before this transition, Fermi arc states can be argued to exist and to lie tangent to the Fermi surface [36].

An aside

To gain a topological understanding of this, we refer to [37]. In this work, the stability of gapless points is determined in terms of attaching to them a topological charge which can be thought of as an element of the $K(\cdot)$ abelian group given to a sphere surrounding the Fermi surface (which is a point in this case). Note that the above work only discusses the Hamiltonians in class A of the Altland-Zirnbauer classification and can be generalized as given in [38].

To avoid confusion, note the above resources talk about the generalized case of interacting systems. In the non-interacting cases where band theory is useful, things get simplified. The topological charge associated to a gapless locus in the Brillouin zone is inferred by surrounding the locus by manifolds over which the family of Hamiltonians is gapped and the classification described in Section 1.2 holds. Usually, this kind of classification of topological (semi-)metals is done by taking the enveloping manifolds to follow the symmetries of the model. However, recent work [39] has suggested some corrections to these classifications done using $K-$theory by taking non-centrosymmetric and more general manifolds around the gapless loci.

3.2 Nodal line semi-metal

Topological Nodal Line Semi-Metals (TNLSMs) [40] can be defined as systems which have a topologically protected bulk gap touching in the form of a co-dimension 2 (recall that for the case of the Weyl semi-metal, it was co-dimension 3) manifold. This locus is usually protected by a crystalline symmetry, such as reflection or inversion.

To diagnose what kinds of topological charges can even be assigned in this case, we look back at $K-$theory. One can determine the classifying space of flattened admissible Hamiltonians $Q(\vec{k})$ in the case of inversion symmetry to be the real Grassmanian, or,

$$Q(\vec{k}) \in \frac{O(m+n)}{O(m) \oplus O(n)} \tag{3.7}$$

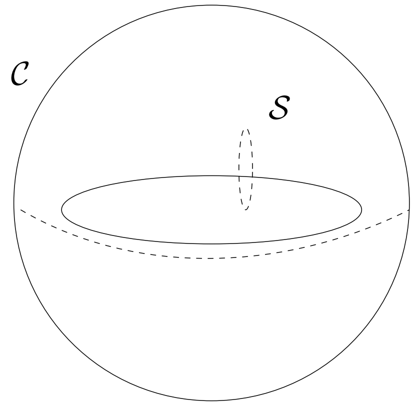

Figure 3.3: Nodal line semi-metal with the curves for the two charges encapsulated.

There appear to be two distinct type of charges that can be associated to this gap touching since

$$\pi_1\left(\frac{O(m+n)}{O(m)\oplus O(n)}\right)=\pi_2\left(\frac{O(m+n)}{O(m)\oplus O(n)}\right)=\mathbb{Z}_2 \tag{3.8}$$

Note that there are various subtleties that arise in the case of finite band systems where the classification and charge assignment can change [39].

One can write a low-energy Bloch Hamiltonian exhibiting a nodal-line to be

$$\mathrm{h}(\vec{k})=(m-k^2)\sigma^3+k_z\sigma^1 \tag{3.9}$$

For this, one can define the two charges as follows:

$$\zeta_1=\oint_{\mathcal{S}}\mathcal{A}dk \tag{3.10}$$

$$\zeta_2=\oint_{\mathcal{C}}\mathcal{F}dk \tag{3.11}$$

where C signifies any loop interlinking the nodal ring and S signifies any co-dimension 1 surface enveloping the locus.

Performing a similar analysis as before, we find a drumhead shaped locus surrounded by the ring for the edge modes. To understand how one can infer the topological behavior of this semi-metal through the action and subsequently, experiments, we refer to [41, 42] where it is put in the broader context of generalized Luttinger theorems.

3.3 $\mathbb{R}P^2$ model

The Chern number was what topologically charged the Weyl nodes in Section 3.1; this invariant was originally described in the context of a spin in the magnetic field, as discussed extensively in Section 1.3.1. We want to check if there is an analogous invariant one can discuss along the lines of [43]. In this case, on the sphere of parametrized ground states as in the original Berry model, one can obtain a gauge invariant phase as one traverses along any trajectory from $\hat{n} \to -\hat{n}$.

Now, we move onto mapping a non-orientable surface into the BZ and asking if this can possibly give us a non-trivial topological invariant. The answer, keeping in spirit with the previous cases, is given by $K(\mathbb{R}P^2) \cong \mathbb{Z}_2$ [44]. A small note: the $K-$theory of non-orientable surfaces always includes a torsion part.

Although topological phases (both SPT and SET phases) involving a non-orientable surface have been talked about previously in literature [45, 46, 47], we want to showcase a simple two-band model while illuminating the edge mode physics, hoping to also give a possible response measurement. On this account, we will be looking at the following model in 3D, which is the UV version of the continuum model suggested in [44]:

$$\mathrm{h}(\vec{k}) = \sum_k \hat{g}(\vec{k}) \cdot \vec{\sigma} \tag{3.12}$$

where

$$g_1(\vec{k}) = \Delta \sin k_z \sin k_x, \;\; g_2(\vec{k}) = -\Delta \sin k_z \sin k_y \tag{3.13}$$

$$g_3(\vec{k}) = -\frac{1}{m}(\cos k_x + \cos k_y) - t \cos k_z + \left(\frac{2}{m} - \mu\right) \tag{3.14}$$

This has inversion symmetry, allowing one to essentially identify the antipodal points on the manifold surrounding the gapless point. $K(S^2/\mathbb{Z}_2 \cong \mathbb{R}P^2)$ being non-trivial would carry over to any inversion symmetric manifold surrounding the gapless loci since any of them could be deformed into each other smoothly.

The invariant in this case that we will be considering is as follows [44, 47]:

$$c_1 = \frac{i}{2\pi} \ln \mathrm{hol}_l(\mathcal{A}) + \frac{1}{2}\frac{i}{2\pi}\int_D \mathrm{tr}\,\mathcal{F} \pmod 1 \tag{3.15}$$

where l is any trajectory on the inversion symmetric manifold connecting $\vec{k}$ and $-\vec{k}$. D is the manifold whose boundary is $l - \bar{l}$ where $\bar{l}$ is the curve obtained by acting the inversion operation on l.

Gapless loci and measuring the charge

For the purpose of simplicity, we will focus on the following parameter regimes: $t = 1, m = 1, \Delta = 1$ and $\mu \in [-1, 5]$. The gapless loci take the form as given in Fig. 3.4 as we tune μ. Each pair of gapless points harbors a $\mathbb{Z}_2$ charge whereas each nodal line

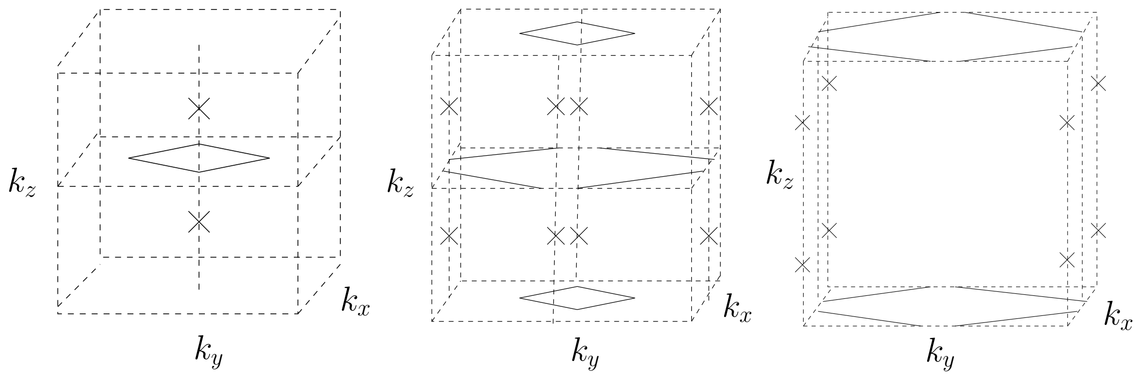

(a) $\mu \in (-1, 1)$ (b) $\mu \in (1, 3)$ (c) $\mu \in (3, 5)$

Figure 3.4: Gapless loci for the $\mathbb{R}P^2$ model with each pair of the crosses, denoting point charges, holding a $\mathbb{Z}_2$ charge. On the other hand, the nodal rings, denoted by solid lines, each hold a $\mathbb{Z}_2$ charge.

contains its own. Turns out that one can formulate an inversion symmetric version of the Nielson-Ninomiya theorem for this case, which is not difficult to see; hence, the overall charge must add to 0, that is, only an even number of charge-bearing entities can exist in the BZ.

Future work

Immediate future work would entail looking at edge mode structuring as we tune some of these parameters. Further, we would want to ideally associate a response to possibly measure the topological nature of the system. Another idea would be to utilise a superconducting Hamiltonian which automatically imposes the $\vec{k} \to -\vec{k}$ identification to avoid double counting. This would discard the requirement of inversion symmetry and give rise to a fully robust topological semi-metal with a novel invariant.

Bibliography

[1] Andreas W W Ludwig. Topological phases: classification of topological insulators and superconductors of non-interacting fermions, and beyond. *Physica Scripta*, 2016(T168):014001, dec 2015.

[2] Alexei Kitaev. Periodic table for topological insulators and superconductors. *AIP Conference Proceedings*, 1134(1):22–30, 05 2009.

[3] P. W. Anderson. More is different. *Science*, 177(4047):393–396, 1972.

[4] E. Fradkin. *Field Theories of Condensed Matter Physics*. Cambridge University Press, 2013.

[5] F. Duncan M. Haldane. Nobel lecture: Topological quantum matter. *Rev. Mod. Phys.*, 89:040502, Oct 2017.

[6] John Michael Kosterlitz. Nobel lecture: Topological defects and phase transitions. *Rev. Mod. Phys.*, 89:040501, Oct 2017.

[7] M. Heyl, A. Polkovnikov, and S. Kehrein. Dynamical quantum phase transitions in the transverse-field ising model. *Phys. Rev. Lett.*, 110:135704, Mar 2013.

[8] A.Yu. Kitaev. Fault-tolerant quantum computation by anyons. *Annals of Physics*, 303(1):2–30, 2003.

[9] Xiao-Liang Qi and Shou-Cheng Zhang. Topological insulators and superconductors. *Rev. Mod. Phys.*, 83:1057–1110, Oct 2011.

[10] M. Z. Hasan and C. L. Kane. Colloquium: Topological insulators. *Rev. Mod. Phys.*, 82:3045–3067, Nov 2010.

[11] Alexander Altland and Martin R. Zirnbauer. Nonstandard symmetry classes in mesoscopic normal-superconducting hybrid structures. *Phys. Rev. B*, 55:1142–1161, Jan 1997.

[12] Davide Gaiotto and Theo Johnson-Freyd. Symmetry protected topological phases and generalized cohomology. *Journal of High Energy Physics*, 2019(5), May 2019.

[13] A. Kitaev. Differential forms on the space of statistical mechanics models. Talk at the conference in celebration of Dan Freed's 60th birthdayhttps://web.ma.utexas.edu/topqft/talkslides/kitaev.pdf, 2019.

[14] Xueda Wen, Marvin Qi, Agnès Beaudry, Juan Moreno, Markus J. Pflaum, Daniel Spiegel, Ashvin Vishwanath, and Michael Hermele. Flow of higher Berry curvature and bulk-boundary correspondence in parametrized quantum systems. *Phys. Rev. B*, 108:125147, Sep 2023.

[15] Po-Shen Hsin, Anton Kapustin, and Ryan Thorngren. Berry phase in quantum field theory: Diabolical points and boundary phenomena. *Phys. Rev. B*, 102:245113, Dec 2020.

[16] Ken Shiozaki. Adiabatic cycles of quantum spin systems. *Phys. Rev. B*, 106:125108, Sep 2022.

[17] Nick G. Jones, Ryan Thorngren, Ruben Verresen, and Abhishodh Prakash. Charge pumps, pivot hamiltonians, and symmetry-protected topological phases. *Phys. Rev. B*, 112:165123, Oct 2025.

[18] A. Kitaev. "Homotopy-theoretic approach to spt phases in action",. talk at Institute for Pure and Applied Mathematics https://www.ipam.ucla.edu/programs/workshops/symmetry-and-topology-in-quantum-matter/, 2015.

[19] Abhishodh Prakash and S. A. Parameswaran. Charge pumps, boundary modes, and the necessity of unnecessary criticality, 2024.

[20] Abhishodh Prakash, Michele Fava, and S. A. Parameswaran. Multiversality and unnecessary criticality in one dimension. *Phys. Rev. Lett.*, 130:256401, Jun 2023.

[21] Shinsei Ryu, Andreas P Schnyder, Akira Furusaki, and Andreas W W Ludwig. Topological insulators and superconductors: tenfold way and dimensional hierarchy. *New Journal of Physics*, 12(6):065010, June 2010.

[22] Xiao-Liang Qi, Taylor L. Hughes, and Shou-Cheng Zhang. Topological field theory of time-reversal invariant insulators. *Physical Review B*, 78(19):195424, November 2008.

[23] Max Karoubi. *K-Theory: An Introduction*, volume 226 of *Grundlehren der mathematischen Wissenschaften*. Springer, Berlin, Heidelberg, 1978.

[24] Adel Bilal. Lectures on anomalies, 2008.

[25] Charles Zhaoxi Xiong. Minimalist approach to the classification of symmetry protected topological phases. *Journal of Physics A: Mathematical and Theoretical*, 51(44):445001, October 2018.

[26] M. J. Rice and E. J. Mele. Elementary excitations of a linearly conjugated diatomic polymer. *Phys. Rev. Lett.*, 49:1455–1459, Nov 1982.

[27] Di Xiao, Ming-Che Chang, and Qian Niu. Berry phase effects on electronic properties. *Rev. Mod. Phys.*, 82:1959–2007, Jul 2010.

[28] János K Asbóth, László Oroszlány, and András Pályi. *A short course on topological insulators*, volume 919. Springer, 2016.

[29] J. E. Avron, R. Seiler, and B. Simon. Homotopy and quantization in condensed matter physics. *Physical Review Letters*, 51(1):51–53, July 1983.

[30] J. E. Avron, L. Sadun, J. Segert, and B. Simon. Topological invariants in fermi systems with time-reversal invariance. *Physical Review Letters*, 61(12):1329–1332, September 1988.

[31] J. E. Avron, L. Sadun, J. Segert, and B. Simon. Chern numbers, quaternions, and berry's phases in fermi systems. *Communications in Mathematical Physics*, 124(4):595–627, December 1989.

[32] Joseph E. Avron, Ruedi Seiler, and Barry Simon. Charge deficiency, charge transport and comparison of dimensions. *Communications in Mathematical Physics*, 159(2):399–422, January 1994.

[33] Shou-Cheng Zhang and Jiangping Hu. A four-dimensional generalization of the quantum hall effect. *Science*, 294(5543):823–828, October 2001.

[34] N. P. Armitage, E. J. Mele, and Ashvin Vishwanath. Weyl and dirac semimetals in three-dimensional solids. *Rev. Mod. Phys.*, 90:015001, Jan 2018.

[35] Varghese Mathai and Guo Chuan Thiang. Global topology of weyl semimetals and fermi arcs. *Journal of Physics A: Mathematical and Theoretical*, 50(11):11LT01, feb 2017.

[36] F. D. M. Haldane. Attachment of surface "fermi arcs" to the bulk fermi surface: "fermi-level plumbing" in topological metals, 2014.

[37] Petr Hořava. Stability of fermi surfaces and k theory. *Phys. Rev. Lett.*, 95:016405, Jun 2005.

[38] Y. X. Zhao and Z. D. Wang. Topological classification and stability of fermi surfaces. *Phys. Rev. Lett.*, 110:240404, Jun 2013.

[39] Faruk Abdulla, Ganpathy Murthy, and Ankur Das. Internal symmetry protected stable topological semimetals in three dimensions. *Phys. Rev. B*, 112:205111, Nov 2025.

[40] Chen Fang, Hongming Weng, Xi Dai, and Zhong Fang. Topological nodal line semimetals. *Chinese Physics B*, 25(11):117106, November 2016.

[41] Chong Wang, Alexander Hickey, Xuzhe Ying, and A. A. Burkov. Emergent anomalies and generalized luttinger theorems in metals and semimetals. *Phys. Rev. B*, 104:235113, Dec 2021.

[42] L. Gioia, Chong Wang, and A. A. Burkov. Unquantized anomalies in topological semimetals. *Phys. Rev. Res.*, 3:043067, Oct 2021.

[43] J M Robbins and M V Berry. A geometric phase for m=0 spins. *Journal of Physics A: Mathematical and General*, 27(12):L435, jun 1994.

[44] Ken Shiozaki, Masatoshi Sato, and Kiyonori Gomi. Topological crystalline materials: General formulation, module structure, and wallpaper groups. *Phys. Rev. B*, 95:235425, Jun 2017.

[45] AtMa P O Chan, Jeffrey C Y Teo, and Shinsei Ryu. Topological phases on non-orientable surfaces: twisting by parity symmetry. *New Journal of Physics*, 18(3):035005, mar 2016.

[46] Marvin Qi, David T. Stephen, Xueda Wen, Daniel Spiegel, Markus J. Pflaum, Agnès Beaudry, and Michael Hermele. Charting the space of ground states with tensor networks. *SciPost Phys.*, 18:168, 2025.

[47] Z. Y. Chen, Shengyuan A. Yang, and Y. X. Zhao. Brillouin klein bottle from artificial gauge fields. *Nature Communications*, 13(1):2215, 2022.

[48] Anatolij Timofeevič Fomenko and Dmitrij Borisovič Fuks. *Homotopical topology*, volume 273. Springer, 2016.

[49] S. MERKULOV. Hatcher, a.algebraic topology (cambridge university press, 2002), 556 pp., 0 521 79540 0 (softback), £20.95, 0 521 79160 x (hardback), £60. *Proceedings of the Edinburgh Mathematical Society*, 46(2):511–512, 2003.

[50] Fabian H. L. Essler, Holger Frahm, Frank Göhmann, Andreas Klümper, and Vladimir E. Korepin. *The One-Dimensional Hubbard Model*. Cambridge University Press, 2005.

[51] Demonstration of the "luttinger liquid" character of bethe-ansatz-soluble models of 1-d quantum fluids. *Physics Letters A*, 81(2):153–155, 1981.

[52] Non-integrable aspects of the multi-frequency sine-gordon model. *Nuclear Physics B*, 516(3):675–703, 1998.

[53] Ian Affleck. Edge magnetic field in the xxz spin-chain. *J. Phys. A: Math. Gen.*, 31(12):2761, mar 1998.

[54] Anna Keselman and Erez Berg. Gapless symmetry-protected topological phase of fermions in one dimension. *Phys. Rev. B*, 91:235309, Jun 2015.

[55] P. Lecheminant, Alexander O. Gogolin, and Alesander A. Nersesyan. Criticality in selfdual sine-Gordon models. *Nucl. Phys. B*, 639:502–523, 2002.

Appendix A

Mathematical Preliminaries

A.1 Some Definitions

Most of these definitions and theorems can be found in [48, 49] and other standard algebraic topology textbooks.

Definition 1: *Given two pointed topological spaces* (X, x_0) *and* (Y, y_0)*, the wedge sum* $(X \vee Y)$ *can be defined to be* $(X \sqcup Y)/\{x_0, y_0\}$*. That is, the disjoint union* $X \sqcup Y$ *formed by identifying* x_0 *with* y_0*.*

Definition 2: *Given two pointed topological spaces* (X, x_0) *and* (Y, y_0)*, the smash product* $(X \wedge Y)$ *can be defined as* $(X \times Y)/(X \vee Y)$*. It can also be seen as* $(X \times Y)/((X \times \{y_0\}) \cup (Y \times \{x_0\}))$*.*

Definition 3: *Given a topological space* X*, we construct its* ***suspension*** SX *by first taking the product topological space* $X \times I$*, where* $I = [0, 1]$*, and identifying* $X \times \{0\}$ *and* $X \times \{1\}$ *to a pt each.*

Definition 4: *Given a pointed topological space* X*, we define its reduced suspension* ΣX *to be formed from* SX *by further identifying* $\{x_0\} \times I$ *to a pt. It can also be viewed as* $S^1 \wedge X$*.*

Definition 5: *The* $n-th$ *homotopy group of a pointed topological space* (X, x_0) *is the set of pointed homotopy classes of maps from* (S^n, s_0) *to* (X, x_0)*, denoted by* $\langle S^n, X \rangle$*.*

Construction 1: *Given pointed topological spaces* (X, x_0) *and* (Y, y_0)*, we can form the space* $Map_\star(X, Y)$ *of pointed maps from* (X, x_0) *to* (Y, y_0)*, endowed with compact open topology.*

Note 1: *A pointed homotopy can alternatively be defined to be a path in the space*

$Map_\star(X,Y)$. In this context, $\langle X,Y\rangle$ can be described as the sets of path components of $Map_\star(X,Y)$.

Definition 6: *The loop space ΩY of a pointed topological space (Y, y_0) is defined to be the space $Map_\star((S^1, s_0),(Y, y_0))$. Intuitively, it is the space of loops in Y based at y_0.*

Definition 7: *The loop space functor $\Omega : Top_\star \to Top_\star$ is a covariant functor that maps each object (X, x_0) in $Top_\star$, the loopspace ΩX, and to each pointed map $f : (X, x_0) \to (Y, y_0)$ the morphism $\Omega f : \Omega X \to \Omega Y$ given by composition with f. For example, it sends a loop $l : (S^1, s_0) \to (X, x_0)$ in (X, x_0) to the loop $f \circ l : (S^1, s_0) \to (Y, y_0)$ in (Y, y_0).*

Definition 8: *If G a topological group, there exists a covariant functor B such that BG, known as a classifying space for G, is a space equipped with a universal principal G-bundle*

$$G \to EG \to BG \tag{A.1}$$

For any sufficiently nice space X, $\{Principal\ G{-}bundles\ over\ X\} \cong [X, BG]$. It can also be shown that BG exists and is unique up to homotopy equivalence.

A.2 Cohomology theories and Ω-spectra

Ω−spectrum

An $\Omega-$spectrum is a family of pointed topological spaces,

$$\dots, F_{-2}, F_{-1}, F_0, F_1, F_2, \dots$$

together with pointed homotopy equivalences

$$F_n \xrightarrow{\sim} F_{n+1}$$

Brown Representability Theorem

Every $\Omega-$spectrum $(F_n)_{n\in\mathbb{Z}}$ defines a reduced generalized cohomology theory $\tilde{h}$ according to

$$\tilde{h}^n(X) := \langle X, F_n\rangle \tag{A.2}$$

Further, conversely, every reduced generalized cohomology theory can be represented by an $\Omega-$spectrum.

Note 2: The unreduced generalized cohomology theory h follows a subset of the full set of axioms implied from the Eilenberg-Steenrod axioms for the homology dual.

Using the Eilenberg-Maclane spectrum forces the following set of homology theories to follow the full set, giving rise to what are now known as ordinary cohomology theories. The axiom omitted is the following::

Dimension axiom: *Let P be the one-point space. Then $H_n(P) = 0 \ \forall \ n \neq 0$.*

A.3 TQFT and Cobordisms

Let M be a $(d+1)-$dimensional oriented manifold of spacetime with Σ defining a spatial slice, with the orientation induced from that of M.

1. To each $d-$dimensional slice Σ, we associate a complex Hilbert space $V(\Sigma)$. This is only dependent on the topology of Σ.
2. The Hilbert space of $\Sigma \sqcup \Sigma'$ is given by
$$V(\Sigma \sqcup \Sigma') = V(\Sigma) \otimes V(\Sigma') \tag{A.3}$$
Consequently, $V(\phi) = \mathbb{C}$ since $\mathbb{C} \otimes V(\Sigma) = V(\Sigma)$.
3. If Σ is the boundary of M, we associate an element $Z(M) \in V(\partial M)$ to the manifold M. Inferring $V(\Sigma)$ as the subspace of ground states, then $Z(M)$ can be thought of as a particular wavefunction. Further, if M is closed, we note that the TQFT associates a complex number to M.
4. $V(\Sigma^\star) = V(\Sigma)^\star$ where $\Sigma^\star$ is Σ with the reversed orientation and $V(\Sigma)^\star$ represents the dual space of $V(\Sigma)$.

Given two manifolds with $\partial M = (\partial M')^\star = \Sigma$, we *glue* these together by taking an inner product of the corresponding states:
$$Z(M \cup_\Sigma M') = \langle \psi' | \psi \rangle \tag{A.4}$$
for $|\psi\rangle \in Z(M)$ and $\langle \psi'| \in Z(M')$. Without proof, we state that if two manifolds together form the boundary of another manifold, they can be considered the *'same'*. That is, if Σ_1 and Σ_2 are such that $\partial M = \Sigma_1 \sqcup \Sigma_2^\star$, we say that Σ_1 and Σ_2 are cobordant.

This means that we can write
$$Z(M) = \sum_{\alpha,\beta} \mathcal{U}^{\alpha\beta} |\psi_{1,\alpha}\rangle \otimes \langle \psi_{2,\beta}| \tag{A.5}$$
where $\{|\psi_{1,\alpha}\rangle$ and $\{|\psi_{2,\beta}\rangle$ form bases for the states in $V(\Sigma_1)$ and $V(\Sigma_2^\star)$ respectively and $\mathcal{U}^{\alpha\beta}$ are unitary coefficients.

The basic idea of a TQFT is that it gives a compact orientable manifold with an invariant. Turns out that a good invariant to be associated to such manifolds is the familiar partition function.

Appendix B

Bosonisation

We now look at the Hamiltonian:

$$\mathrm{H} = \sum \frac{(1+(-1)^j\delta)}{2}(c_j^\dagger c_{j+1} + h.c) + J\sum(-1)^j c_j^\dagger c_j + U\sum\left(n_j - \frac{1}{2}\right)\left(n_{j+1} - \frac{1}{2}\right) \tag{B.1}$$

We want to understand what happens to the texture when $U \neq 0$. We start with $\delta = J = 0$. Using bosonization, we obtain the following field-theoretic description [50]:

$$\mathrm{H} = \frac{v}{2\pi}\int d^2x \left[\frac{1}{4K}(\partial_x\phi)^2 + K(\partial_x\theta)^2\right] \tag{B.2}$$

where ϕ is a compact boson field, that is, $\phi = \phi + 2\pi$; also, K is the Luttinger parameter. Note that this gives us a conformal manifold, each K giving us a distinct CFT (the scaling dimensions of the operators are dependent on K). Since when $U = 1$ and $\delta = J = 0$ the model is exactly solvable using the Bethe ansatz [51], we can find the corresponding Luttinger parameter in terms of U:

$$K = \frac{\pi}{2\arccos(-U)} \tag{B.3}$$

This makes sense as when $U = 0$, we get $K = 1$ as expected for a non-interacting theory. Also note that this only holds when $|U| < 1$ as is apparent with the form.

B.1 Preliminaries

One can obtain the CFT Hamiltonian *Eq.* (B.2) through standard bosonization techniques [50]. Here, ϕ and θ are conjugate fields. The Luttinger parameter sets the scaling dimensions $[X_{\alpha\beta}]$ of local and non-local operators $X_{\alpha\beta}$ as follows:

$$X_{\alpha\beta} = e^{i(\alpha\phi+\beta\theta)} \implies [X_{\alpha\beta}] = \alpha^2 K + \frac{\beta^2}{4K} \tag{B.4}$$

When α, β are integers, they are local and when rational, non-local.

We will mainly focus on what happens as we perturb away from the gapless phase. We first introduce the δ (bond dimerization) term. The bosonized form of this adds to the Hamiltonian as

$$2\mathcal{AC} \int dx \cos\phi \tag{B.5}$$

where $\mathcal{A}$ and $\mathcal{C}$ are some constants that need to be fitted according to the exact microscopic description. The J term just adds as:

$$\frac{1}{2\pi}\partial_x\phi - (-1)^j \mathcal{B}\sin(\phi) \tag{B.6}$$

where $\mathcal{B}$ is again a constant. Note that in the Hamiltonian we had a $(-1)^j$ coefficient multiplying n_j; taking this into account, we are left with $-\#J\sin(\phi)$ as the leading order contribution from this term.

B.2 Stability of the phase diagram to interactions

Moving away from the origin, we have the leading order contributions from adding the J and δ terms (Eq. (B.5), Eq. (B.6)) as

$$\mathrm{H} = \frac{v}{2\pi}\int d^2x \left[\frac{1}{4K}(\partial_x\phi)^2 + K(\partial_x\theta)^2 + \#\delta\cos(\phi) + \#J\sin(\phi)\right] \tag{B.7}$$

The scaling dimensions of the perturbing operators can be obtained by Eq. (B.4):

$$[\cos(\phi)] = [\sin(\phi)] = [e^{i\phi}] = K \tag{B.8}$$

When $K < 2 \implies U > \frac{-1}{2}$, the operators are relevant, meaning we move away from the gapless phase. As a sanity check, $U = 0$ corresponds to this regime and this matches our expectations. Now, we can find $\langle\phi\rangle$ such that the free energy is minimized. Plotting this as a vector on the phase diagram with the angle given by $\langle\phi\rangle$, we get a vortex. This can be contrasted with the band-theoretic derivation of the same to make the connection to berry phase!

When $K > 2 \implies U < \frac{-1}{2}$, the operators become irrelevant and we remain in the gapless phase as we move away.

When $U > 1$, the corresponding RG term, which can be argued to be $\sim \cos(2\phi)$, becomes relevant. However, the particle-hole symmetry gets explicitly broken as we go away from the $J = 0$ subspace and this term can't appear. Staying in this regime, due to competition with the $\cos(\theta)$ term, we get a first-order diabolical line, terminating in an Ising transition [52] as talked about in [15].

B.3 Stability of edge modes

Now, we shall impose open boundary conditions in the field theoretic description by introducing a fiducial vacuum $\langle\phi\rangle = 0$ at the boundary [53, 54]. Say the bulk has $\langle\phi\rangle = \frac{\pi}{4}$, then to match with the boundary conditions, we need $\langle\phi\rangle$ to deform smoothly so as to minimize the free energy associated with the action. This happens close to the edge.

Now consider $\langle\phi\rangle = \pi$ in the bulk. Now there are two ways to match with the

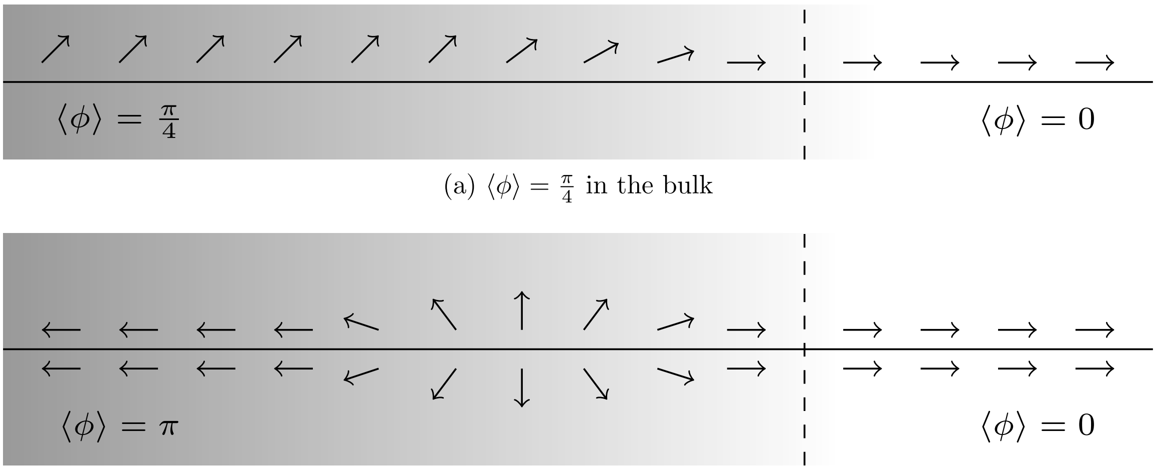

(a) $\langle\phi\rangle = \frac{\pi}{4}$ in the bulk

(b) $\langle\phi\rangle = \pi$ in the bulk

Figure B.1: In (a), there is a non-degenerate way of 'tumbling' to match with the boundary condition whereas in (b) there appears to be a degeneracy.

boundary conditions: degeneracy. Since this doesn't occur with periodic boundary conditions, we can diagnose this being an edge phenomenon. The charge operator acts as

$$\frac{1}{2\pi}\int dx(\partial_x\phi) \tag{B.9}$$

and the edge modes have an integral charge difference, which means that they correspond to truly distinct states. This showcases the stability of the edge modes to interactions.

B.4 Adding μ

The chemical potential term adds as $\mu(\partial_x\phi)$. In the action, we can essentially get rid of this term by completing the square and redefining ϕ: $\langle\phi\rangle \to \langle\tilde{\phi}\rangle$.

Initially, without μ, we had an accidental translation symmetry (in the bosonized picture) of the form:

$$T_a : \phi \to \phi + \pi \tag{B.10}$$

However, this only holds at the origin. More generally, we had $\phi \to \phi + 2\pi$ symmetry. But in the language of the compact boson, this isn't a symmetry but a gauge redundancy. Now, including μ, we get an accidental symmetry of the form

$$\tilde{T}_a : \tilde{\phi} \to \tilde{\phi} + 2k_F \tag{B.11}$$

at the origin; correspondingly, we have a true symmetry of

$$\tilde{T} : \tilde{\phi} \to \tilde{\phi} + 4k_F \tag{B.12}$$

Since k_F is irrational, there is no trigonometric function following this symmetry in $\tilde{\phi}$. This means that the relevant operators from before are not allowed in the action under the RG flow: gapless phase persists even slightly away.

B.5 Adding a superconducting term

The superconducting term $\sum(\Gamma c_j^\dagger c_{j+1}^\dagger + h.c)$ occurs as proportional to $\cos(2\theta + \gamma)$ (where $\Gamma = |\Gamma|e^{i\gamma}$) in the Hamiltonian Eq. (B.2). This has a scaling dimension of $\frac{1}{K}$, meaning that it is relevant when $K > 2$.

However, note that there are other contributions in the action coming from the δ and J terms. Since this is always greater than the others very close to the gapless point $\delta \sim J \sim 0$, there is an immediate transition into a superconducting phase. But going further, the δ and J terms dominate, giving rise to the texture from prior.

Now, when these two are similar to each other, one can show that this becomes gapless again and we encounter an Ising critical CFT [55].

B.5.1 Asymmetry of the texture

Clearly, the texture on the phase diagram seems to be asymmetric under $\delta \to -\delta$; this is not a bug! This can be seen by probing the limits $J \to \pm\infty$.

As we take the positive limit, we get $\hat{d}$ mapping to the north pole $(0, 0, 1)$ $\forall$ k which would then give rise to a solid angle of 0. We get similar behavior when we take the negative limit, retaining the vanishing solid angle. This means that as we go farther away from the diabolical point, the angle of the arrow constituting the texture, which is indeed given by the Berry phase, at $\delta = 0$ both sides of the y-axis flattens to be

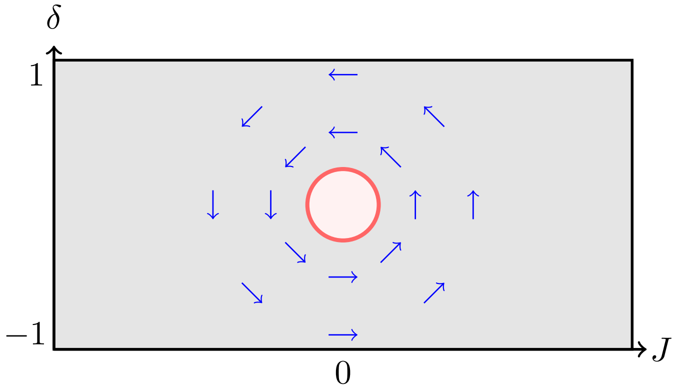

Figure B.2: The phase diagram where the filled red region signifies the superconducting phase and the dark red outline corresponds to the transition. One can notice the texture still persisting in the gray insulating phase.

close to 0.

Since we know that the winding number is unit in this case, we expect that in this limit, there shouldn't be any further "winding" of the arrows after we encounter the $\theta = \pi$ axis (θ is the parameter for the loop in the phase diagram). Hence, the asymmetry makes sense, noting that at $\theta = \frac{\pi}{2}$, $\gamma = \pi$. A similar effect for a similar reason is seen in the $d = 2$ case.

Note that since the bosonisation results only hold close to the diabolical point, we can rest assured that the agreement is still preserved.

Appendix C

Numerical study

One of the advantages of our results is that they can be implemented in numerical studies easily. In particular, the integral expressions in Eqs. (2.32) and (2.35) can be efficiently approximated without the need to ensure smooth gauge choices as we will demonstrate in this section.

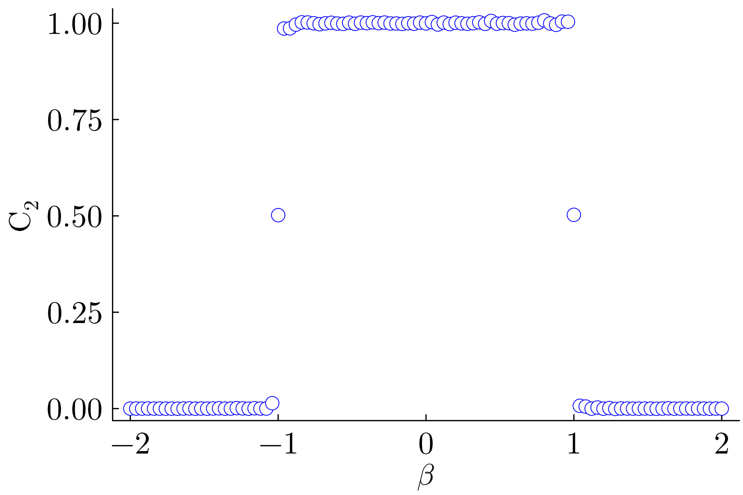

Figure C.1: The expression for C_2 in Eq. (2.32) evaluated using Monte Carlo integration for 10^6 steps.

For the calculations in this section, let us use spherical polar coordinates $\theta_{1,2,3} \in [0, \pi)$, $\phi \in [0, 2\pi)$ to represent the parameter space S^3 as

$$\begin{pmatrix} n_1 \\ n_2 \\ n_3 \\ n_4 \end{pmatrix} = \begin{pmatrix} \cos\theta_1 \\ \sin\theta_1 \cos\theta_2 \\ \sin\theta_1 \sin\theta_2 \cos\phi \\ \sin\theta_1 \sin\theta_2 \sin\phi. \end{pmatrix} \tag{C.1}$$

We will represent the Brillouin zone by the momentum $k \in [0, 2\pi)$ as usual. Let us begin with recasting the integrand in Eqs. (2.32) and (2.35) into a more practical form for implementation on a computer.

$$\epsilon_{abcde}\epsilon^{\mu\nu\alpha\beta}\hat{g}^a\partial_\mu\hat{g}^b\partial_\nu\hat{g}^c\partial_\alpha\hat{g}^d\partial_\beta\hat{g}^e = \begin{vmatrix} \hat{g}_1 & \partial_{\theta_1}\hat{g}_2 & \partial_{\theta_2}\hat{g}_3 & \partial_\phi\hat{g}_4 & \partial_k\hat{g}_1 \\ \hat{g}_2 & \partial_{\theta_1}\hat{g}_3 & \partial_{\theta_2}\hat{g}_4 & \partial_\phi\hat{g}_5 & \partial_k\hat{g}_1 \\ \hat{g}_3 & \partial_{\theta_1}\hat{g}_4 & \partial_{\theta_2}\hat{g}_5 & \partial_\phi\hat{g}_1 & \partial_k\hat{g}_2 \\ \hat{g}_4 & \partial_{\theta_1}\hat{g}_5 & \partial_{\theta_2}\hat{g}_1 & \partial_\phi\hat{g}_2 & \partial_k\hat{g}_3 \\ \hat{g}_5 & \partial_{\theta_1}\hat{g}_1 & \partial_{\theta_2}\hat{g}_2 & \partial_\phi\hat{g}_3 & \partial_k\hat{g}_4 \end{vmatrix} \tag{C.2}$$

Eq. (C.2) inserted into Eqs. (2.32) and (2.35) can be evaluated efficiently, e.g. using Monte-Carlo. We demonstrate this in this section using variants of the model in Eqs. (2.56) to (2.58).

C.1 Computing the Chern number

Let us begin with a calculation of the Chern number. By construction, we expect this to evaluate to a non-zero value for the model in Eqs. (2.56) to (2.58). This number is quantized, it is instructive to study deformations of Eqs. (2.56) to (2.58) where we can observe an abrupt transition. To do see this, let us introduce a one-parameter deformation as follows

$$\mathrm{H}_1(\hat{n},\beta) = \mathrm{H}_1(\hat{n}) + \beta\sum_{x\in\mathbb{Z}}(-1)^x c^\dagger_\alpha(x)\sigma^1_{\alpha\beta}c_\beta(x). \tag{C.3}$$

This corresponds to the same form as in Eq. (2.58) with the modification $g_1 \mapsto g_1 + \beta$. For $\beta = 0$, we expect $\mathsf{C}_2 = 1$ and for $\beta \to \infty$, we get a trivial family and thus, expect $\mathsf{C}_2 = 0$. For $\beta = \pm 1$, we see that the Hamiltonian family in Eq. (C.3) encounters a gap closing point since $g_1 \mapsto 0$ for $n_1 = \mp 1$ when

$$\mathrm{H}_1 = \frac{1}{2}\sum_{x\in\mathbb{Z}}\sum_{\alpha\in\uparrow,\downarrow}\left(c^\dagger_\alpha(x)c_\alpha(x+1) + h.c.\right). \tag{C.4}$$

The gapless ground state of Eq. (C.4) consists of partially filled bands of a spinful fermion and represents a 'phase transition' between distinct topological families with different Chern number values. This is clearly verified numerically in Fig. C.1.

C.2 Computing the geometric invariant

The calculation of the geometric phase is similarly done using Monte-Carlo methods by performing the integral over the relevant sub-manifold $\mathcal{M}_3$. Hence, we have shown that the topological family of states exhibit non-trivial topological properties.

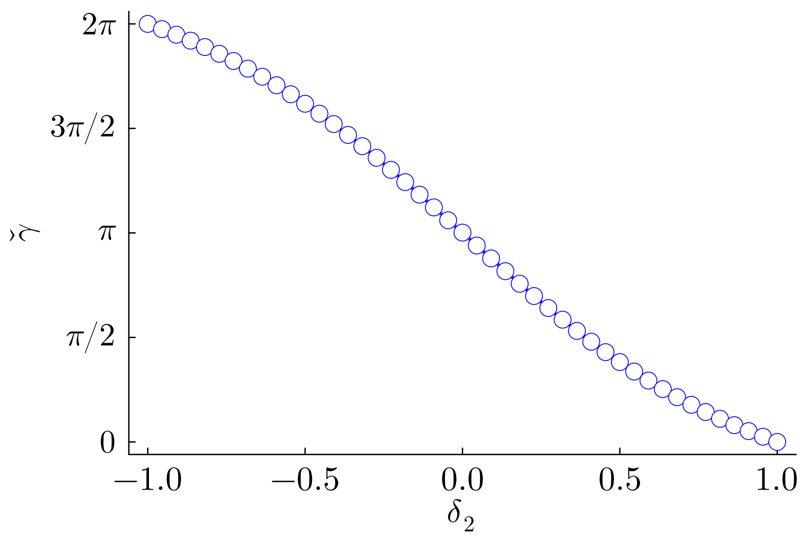

Figure C.2: The expression for Higher Berry phase $\check{\gamma}$ in Eq. (2.35) evaluated for parametric S^2 slices at various fixed latitudes of S^3 obtained by fixing one of the polar coordinates θ_1 using Monte-Carlo integration with 10^5 steps.

Appendix D

Suspension construction

For the sake of the construction recipe, we assume that Kitaev's conjecture as described in Section 1.2.3. holds. To fit the purpose of this chapter, we reduce the conjecture to the following perspective: after fixing the system to be either bosonic or fermionic and claiming it to be $G-$symmetric, we have E_d which is defined to be the space of all d-dimensional gapped invertible states. Then,

$$E_d \simeq \Omega E_{d+1} \tag{D.1}$$

$$E^d(X) := [X, E_d] \tag{D.2}$$

where $[X, E_d]$ is the set of homotopy classes of maps from X to E_d. The above expectation that there is such a generalised cohomology theory E^d, describing the space of invertible ground states is enough for us to make the following statement.

Let (X, x_0) be a pointed topological space, then

$$E^d(X) \cong \tilde{E}^d(X) \oplus E^d(\{x_0\}) \tag{D.3}$$

where the total classification splits into a direct sum over two terms the former of which discusses the phases over the space X that don't come from constant families. The latter includes in it all the ordinary d-dimensional phases. Note that this includes topological phases, etc.

Freudenthal suspension theorem [49] tells us that (the usual form of the theorem can be brought to this by using the definition of our generalized cohomology theory)

$$\tilde{E}^d(X) \cong \tilde{E}^{d+1}(SX) \tag{D.4}$$

for nice enough spaces.

Using this along with Eq. (D.3) gives us

$$E^d(S^n) \cong \tilde{E}^{d-n}(S^0) \oplus E^d(\{x_0\}) \cong E^{d-n}(\{x_0\}) \oplus E^d(\{x_0\}) \tag{D.5}$$

D.1 Recipe

Let s_d be a $d-$dimensional gapped invertible system over a q-dimensional parameter space X, with an inverse $\bar{s}^{[d]}$. We now construct the non-trivial $(d+1)$-dimensional system Ss_d parametrized over SX by alternatively stacking $s^{[d]}$ and $\bar{s}_d$ along the new spatial dimension, say x_{d+1}. As shown in Fig. D.1, along the new parameter λ_{q+1},

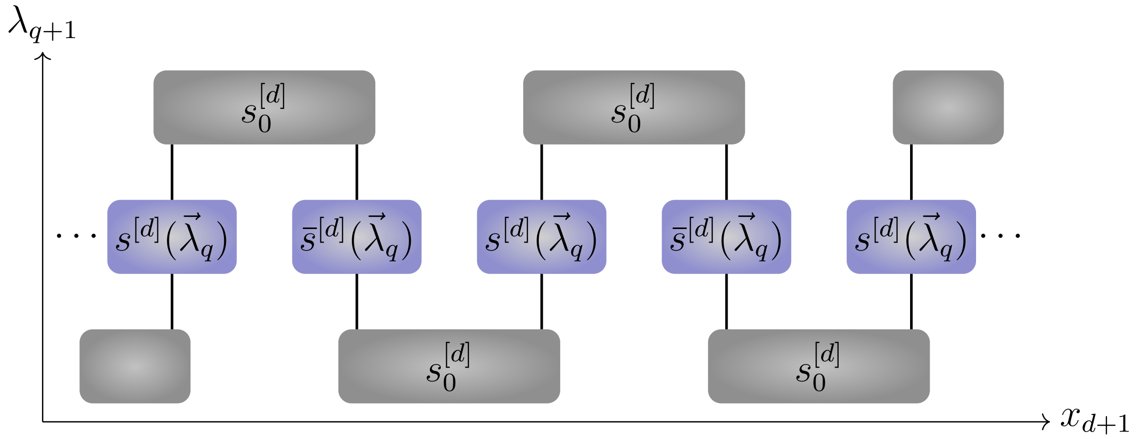

Figure D.1: The suspension construction taking the new parameter to be λ_{q+1}.

continuously deform alternating $s^{[d]}$ and $\bar{s}^{[d]}$ into trivial families. This implies that, if say $\lambda_{q+1} \in [-1, 1]$, then the (now) $s^{[d+1]}$ family at the boundary slices is trivial.

Appendix E

Anomaly classification

This section will mostly deal with Bosonic SPTs, generalizing to fermionic cases requires some more machinery owing to attributing a *spin* structure to manifolds. We dive into this with an example; consider the following nontrivial SPT phase protected by a $\mathbb{Z}_2 \times \mathbb{Z}_2$ symmetry, the Haldane phase

$$\mathrm{H} = -\sum_{j=1}^{N-1} Z_j X_{j+\frac{1}{2}} Z_{j+1} - \sum_{j=1}^{N} Z_{j-\frac{1}{2}} X_j Z_{j+\frac{1}{2}} \tag{E.1}$$

where each of the $\mathbb{Z}_2 \times \mathbb{Z}_2$ symmetry sectors are generated by

$$U^{(1)} = \prod_{j=1}^{N} X_j,\ U^{(2)} = \prod_{j=1}^{N+1} X_{j-\frac{1}{2}} \tag{E.2}$$

Since the Hamiltonian is made of commuting terms, the ground state is given by

$$Z_j X_{j+\frac{1}{2}} Z_{j+1} |\psi\rangle = |\psi\rangle,\ Z_{j-\frac{1}{2}} X_j Z_{j+\frac{1}{2}} |\psi\rangle = |\psi\rangle \tag{E.3}$$

Using this, we verify that the symmetry transformations only act as boundary operators on ground state manifolds

$$U^{(1)} = \prod_{j=1}^{N} Z_{\frac{1}{2}} \otimes Z_{N+\frac{1}{2}},\ U^{(2)} = \prod_{j=1}^{N} X_{\frac{1}{2}} Z_1 \otimes Z_N X_{N+\frac{1}{2}} \tag{E.4}$$

Note that the symmetry acts as a nontrivial projective representation on each boundary characterized by $\omega \in \mathcal{Z}^2(\mathbb{Z}_2 \times \mathbb{Z}_2, U(1))$.

To understand the emergence of the t' Hooft anomaly, we look at the partition function of the boundary of a half infinite chain with background gauge field. This is a $(0+1)-$dimensional object. Our Euclidean partition function on a circle is just

$$\mathrm{tr}_{\mathcal{H}}(e^{-\beta H}) \tag{E.5}$$

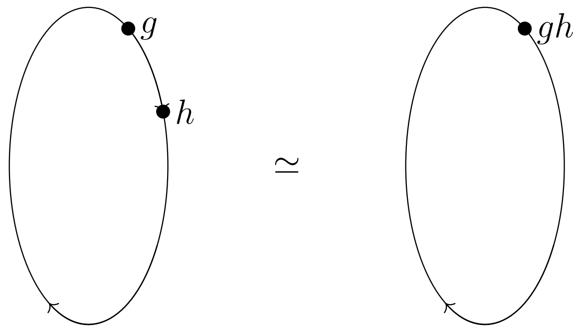

Figure E.1: Two gauge equivalent configurations on the $(0+1)-$dimensional boundary.

However, introducing background gauge fields means imposing twisted boundary conditions. Incorporating this, we have

$$Z[\partial M, A] = \mathrm{tr}_{\mathcal{H}}[U^{(g)} e^{-\beta H}] \tag{E.6}$$

Take two configurations on the boundary that are gauge equivalent, say as given in Fig. E.1. The partition functions are however connected by a factor $\omega(g,h)^{-1}$

$$\mathrm{tr}_{\mathcal{H}}[U^{(g)} U^{(h)} e^{-\beta H}] = \omega(g,h)^{-1}\, \mathrm{tr}_{\mathcal{H}}[U^{(gh)} e^{-\beta H}] \tag{E.7}$$

This is completely due to the fact that symmetries act projectively on the boundary:

$$U(g)U(h) = \omega(g,h)^{-1} U(gh) \tag{E.8}$$

This ambiguity can't be canceled by adding a local counter-term at the boundary. It at most removes the co-boundaries of the symmetry representation. This means that the boundary partition function when viewed by itself has a phase ambiguity. There is one way to get rid of it: by looking at the boundary as a part of the higher dimensional bulk. For this, we need the bulk topological action.

Note: the long-distance limit of gapped theories are conjectured to being Topological Quantum Field Theories (TQFT). These are a subset of QFTs that can surprisingly be given a rigorous mathematical backing. In our case, it is even more special: SPTs correspond to invertible topological field theories in the same limit, that is, the partition function is just a pure phase. For Atiyah's axioms defining the same, we refer to Section A.3. Now we know that one can associate an invariant in the name of the partition function to an oriented manifold. For the case of a triangulated manifold, where one defines $Z(M)$ via a state-sum on triangulation, the Dijkgraff-Witten invariant seems to be useful in constructing one such partition function. Such TQFTs are known to be Dijkgraff-Witten theories. Further note that these are discrete (gauge) group analogues of the Chern-Simons theories.

Following this spirit, we construct the topological action by first triangulating M, which is now an oriented closed 2d surface, by giving it a simplicial structure. We attribute group elements of G to live on the $1-$simplices and that the composition of such elements satisfies a flatness condition $g_{01}g_{12} = g_{02}$ for each $2-$simplex. This takes care of representing a flat background $G-$gauge field. We require this since we only want the topological part of the response: we don't want any propagating gauge modes to make their way into the partition function.

We now associate a Boltzmann weight $\omega(g, h)$ on each $2-$simplex. The partition function is subsequently obtained by

$$Z^{\mathrm{DW}}_{(1+1)d}[M, A] = \prod_{\sigma} \omega(g, h)^{\epsilon(\sigma)} \tag{E.9}$$

where ϵ is the orientation of the particular $2-$simplex. Requiring that the theory is purely topological, that is independent of triangulation, implies imposing the following cocycle condition

$$\omega(g, h)\omega(gh, k) = \omega(g, hk)\omega(h, k) \tag{E.10}$$

One can check that the partition function for a closed M is invariant under $\omega \mapsto \omega + \alpha(g)\alpha(gh)^{-1}\alpha(h)$ which means that only $[\omega] \in \mathcal{H}^2(G, U(1))$ matters for specifying a theory up to a local counterterm. By this procedure, the bulk topological action rudimentarily seems like a Dijkgraff-Witten type action although the gauge field is not summed over.

When we just take the boundary, under a gauge transformation between two equivalent configurations as we have seen before, our partition function accumulates a phase ambiguity in terms of $\omega(g, h)^{-1}$ (Eq. (E.7)). When seen as attached to the bulk, such a gauge transformation is realized by adding to the bulk a $2-$simplex with a Boltzmann weight $\omega(g, h)$ in conjunction to the boundary. This exactly cancels the phase ambiguity coming from the boundary. Hence,

$$Z_{(0+1)d}[\partial M, A] Z^{\mathrm{DW}}_{(1+1)d}[M, A] \tag{E.11}$$

is gauge invariant. Hence, the classification of Bosonic SPTs in $(1 + 1)-$dimensions is done by $\mathcal{H}^2(G, U(1))$. This is readily generalized to higher dimensions to consider Bosonic SPTs in $(d + 1)-$dimensions.